

Measurements and Modeling of Photosynthetic Active Radiation (PAR) at a Semi-Mountainous Site in Cyprus



S Pashiardis^{1*}, SA Kalogirou^{1**} and A Pelengaris²

¹Department of Mechanical Engineering and Materials Science and Engineering Cyprus University of Technology, P. O. Box 50329, 3603, Limassol, Cyprus, Tel: +357-2500-2621, Fax: +357-2500-2637, Email: soteris.kalogirou@cut.ac.cy

^{**} Founding Member of the Cyprus Academy of Sciences, Letters, and Arts.

²Department of Cyprus Public Work, Ministry of Transport Communications and Works, Cyprus.

*Corresponding author: S Pashiardis, Department of Mechanical Engineering and Materials Science and Engineering, Cyprus University of Technology, P. O. Box 50329, 3603, Limassol, Cyprus

ARTICLE INFO

Received: 📅 November 22, 2022

Published: 📅 December 06, 2022

Citation: S Pashiardis, S A Kalogirou and A Pelengaris. Measurements and Modeling of Photosynthetic Active Radiation (PAR) at a Semi-Mountainous Site in Cyprus. Biomed J Sci & Tech Res 47(3)-2022. BJSTR. MS.ID.007502.

Keywords: Global Solar and PAR Radiation; Quality Control; Statistical Analysis; fPAR; fFEC; K_{PAR} Indices; Modeling PAR Radiation

ABSTRACT

In this study, hourly measurements of global solar irradiances, photosynthetically active radiation (PAR) and daily sunshine duration are assessed through an extensive quality control procedure and statistical analysis on the measured and derived solar and PAR indices for a semi-mountainous location using data from the last five years (2016-2020). From this analysis the seasonal characteristics of PAR and its derived indices are examined. This information is useful for agronomists and agrometeorologists who are interested in the efficiency of crop productivity and therefore they are interested on the levels of PAR radiation. Monthly mean hourly values of the radiation components are estimated and shown through isoline diagrams. Monthly mean daily PAR generally increased from 13.7 mol/m²/d in December to 49.8 mol/m²/d in July with an annual mean value being 31.4 mol/m²/d. Simultaneously, similar analysis is carried out over various PAR indices estimated on both hourly and daily basis. Monthly mean daily fFEC_d (ratio of daily Photosynthetic Photon Flux Density (PPFD) to daily global irradiation) increased from 1.77 mol/MJ in April to 1.83 mol/MJ in January with an annual mean value being 1.80 mol/MJ. Clearness index (K_t) was used for characterizing sky conditions, and it was discovered that clear skies represent 40.4 % of the days in a year, while cloudy conditions are recorded in 12.2 %. Generally, fFEC_d is decreased from 1.91 mol/MJ under cloudy conditions to 1.77 mol/MJ under clear sky conditions, which is due to the strong absorption and scattering effects of clouds on longer wavelengths. The annual average of daily clearness index (K_t) is 0.565 with a standard deviation of 0.161. One linear and one multilinear model as well as three power law models were tested and validated under all sky conditions. The best performance was obtained from the linear relationship between PPFD and global irradiance, while the second one was the multiple regression model based on global irradiance and clearness index. The rest four models use power law equations based mainly on clearness index, optical air mass and cosine of solar zenith angle. All the models showed high coefficients of determination (R^2) which are closed to 1.

Abbreviations: AF_{clear} : Ratio of PARE clear to the extraterrestrial one (PARE₀); AST: Apparent Solar Time (hour); B_n : Hourly normal beam irradiance (W/m²); c: Correction for summer time (c=1 for summer and c=0 for winter); CDF: Cumulative density function; CV: Coefficient of variation (%); d_n : Day number of the year (1..365); e_a : Screen level actual water vapour pressure (kPa or hPa); e_s : Saturated screen level water vapour pressure (kPa or hPa); E_t : Estimated irradiance (W/m²); E_t : Equation of time (min); ERL: 'Extremely rare' (ERL) limits (W/m²); fFEC: Hourly fraction of PPFD to global radiation (μmol/J); fFEC_d: Daily fraction of PPFD_d to global irradiation

(G_d) (mol/MJ); $fPAR$: Hourly fraction of PARE to global radiation; $fPAR_d$: Daily fraction of PARE to global radiation (G_d); G : Hourly global solar irradiance (W/m^2); G_d : Daily global solar irradiance (MJ/m^2); G_o : Hourly Extraterrestrial horizontal irradiance (W/m^2); G_{od} : Daily extraterrestrial irradiation (ETR) (MJ/m^2); G_c : Clear-sky global solar irradiance (W/m^2); G_{cd} : Daily global irradiation for clear-sky conditions (MJ/m^2); G_{sc} : Solar constant ($1367 W/m^2$); G_{max} : Highest daily global solar irradiance (W/m^2); k_{PAR} : Hourly PAR Clearness index ($PARE/PARE_o$); K_{PAR} : Daily PAR Clearness index ($PARE_d/PARE_{od}$); k_i : Hourly clearness index (G/G_o); K_T : Daily clearness index (G_d/G_{od}); LF : Conversion factor for PAR irradiance ($4.57 \mu mol s^{-1} W^{-1}$) (McCree, 1972); m : Optical air mass; M_i : Measured irradiance (W/m^2); MBE : Mean Bias Error; MMH : Mean Monthly Hourly; n : Number of observations; N : Number of days; $PARE$: Hourly Photosynthetic Active Irradiance (W/m^2); $PARE_d$: Daily Photosynthetic Active Irradiation (MJ/m^2); $PARE_{sc}$: PAR Solar constant ($534.6 W/m^2$); $PARE_o$: Hourly Photosynthetic Active Irradiance at the top of the atmosphere (W/m^2); $PARE_{od}$: Daily Photosynthetic Active Irradiation at the top of the atmosphere (MJ/m^2); $PPFD$: Hourly Photosynthetic Photon Flux Density ($\mu mol s^{-1} m^{-2}$); $PPFD_{clear}$: Hourly Photosynthetic Photon Flux Density under clear sky ($\mu mol s^{-1} m^{-2}$); $PPFD_x$: Maximum hourly Photosynthetic Photon Flux Density ($\mu mol s^{-1} m^{-2}$); $PPFD_o$: Hourly extra-terrestrial Photosynthetic Photon Flux Density ($\mu mol s^{-1} m^{-2}$); $PPFD_{od}$: Daily extrterrestrial Photosynthetic Photon Flux Density ($mol m^{-2} d^{-1}$); PPL : 'Physically possible' limits (W/m^2); P/P_o : Pressure correction for station height; $Q1$: First Quartile; $Q3$: Third Quartile; R^2 : Coefficient of determination; RE : Relative percentage error (%); RH : Relative humidity (%); $RMSE$: Root Mean Square Error; S : Standard deviation of residuals; S_d : Daily sunshine duration (hours); S_{od} : Astronomical day length (hours); $StDev$: Standard deviation (Std); SW : Shortwave radiation t Local time (hour); $Ta(^{\circ}C)$: Air temperature at screen level ($^{\circ}C$), $Ta(K)=273.16+ Ta(^{\circ}C)$; T_d : Dew point temperature ($^{\circ}C$); VPD : Vapor pressure deficit (kPa or hPa); z : Station's elevation (m)

Greek:

α_s	Solar altitude angle (degrees)
δ	Solar declination angle (degrees)
$\delta_r(m)$	Rayleigh optical depth at air mass m
ε	Correction factor to mean solar distance
θ_z	Solar zenith angle (SZA) (degrees)
λ	Longitude of the station in degrees (East positive)
λ_{ST}	Reference longitude of the time zone in degrees (for Cyprus= 30°)
μ	Cosine of solar zenith angle ($\cos(\theta_z)$)
σ	Relative sunshine duration (S_d/S_{od})
φ	Latitude of the station in degrees
ω	Hour angle (degrees)
ω_s	Sunset hour angle (degrees)

Introduction

Photosynthetically Active Radiation (PAR) is defined as the electromagnetic radiation in the waveband between 400 and 700 nm, which can be used as a source of energy for photosynthesis by green plants [1,2]. PAR is a key parameter in many physical, chemical and biological processes, such as plant physiology, crop growth, biomass production [3,4]. It is a key variable in a wide range of eco-physiological models, both at leaf photosynthesis level [5] and crop production level [6]. Moreover, accurate PAR measurements are important for the determination of deforestation and climate-change impacts on agriculture [7,8]. Meanwhile, reconstruction of PAR during the last decades has gained much scientific interest in China with respect to the global climate-change [9-11]. PAR is expressed either in terms of Photosynthetic Photon Flux Density (PPFD) in units of $\mu\text{mol}/\text{s}/\text{m}^2$, since photosynthesis is a quantum process, or in terms of energy (PARE, Photosynthetically Active Radiation) in units of W/m^2 [12], which is more suitable for energy balance studies. Usually, PPFD is recorded, and converted into energy units according to the McCree conversion factor of $4.57 \mu\text{mol}/\text{J} \pm 3\%$ depending on climatic factors [13]. For the diffuse component, under blue sky an average value of $4.28 \mu\text{mol}/\text{J}$ was reported [14]. In the presence of clouds, the factor increases from $4.24 \mu\text{mol}/\text{J}$ to the value of $4.57 \mu\text{mol}/\text{J}$ under overcast conditions [15].

PAR is measured only in a limited number of stations around the world. This parameter is often indirectly calculated from global horizontal radiation. Therefore, it can be also expressed as (a) a fractional energy of PAR to global radiation ($f\text{PAR}=\text{PARE}/G$), (b) as a fraction of photon flux to the global radiation ($f\text{FEC}=\text{PPFD}/G$) in $\mu\text{mol}/\text{J}$ or in mol/MJ for daily values and (c) as a clearness index ($K_{\text{PAR}}=\text{PARE}/\text{PARE}_0$) i.e., the ratio of PAR to the extraterrestrial PAR irradiance. The ratio $f\text{PAR}$ falls between 0.40 and 0.50 [16,17]. Values above 0.50 occur under very low sun or thick cloud cover [18] Monteith [4] suggested that a constant ratio of 0.50 can be used for practical applications regardless of atmospheric aerosols and water vapor concentrations. Regarding the conversion efficiency ($f\text{FEC}$), it was found that this ratio varies between 1.7 and $2.9 \mu\text{mol}/\text{J}$ [11, 18-22]. This ratio increases with water vapor content and cloud amount but decreases with aerosol loading and the solar zenith angle [20,23]. This fact is attributable to cloud-related absorption and diffusion of solar radiation across different regions of the spectrum. The presence of water vapor increases the absorption effects within the infrared region of the spectrum, decreasing broadband solar irradiance levels to a greater extent than PAR. A secondary effect of water content is the enhancement of aerosol-related diffusion, which affects PAR more than broadband solar irradiance [18]. The fraction of PAR to the extraterrestrial irradiance at the top of the atmosphere is about 0.46 [24]. The solar visible constant is $534.6 \text{W}/\text{m}^2$ [25] which is equivalent to the value of PPFD_{sc} of $2443.3 \mu\text{mol}/\text{s}/\text{m}^2$.

The definition of sky types (clear, partly cloudy and overcast) is mainly based on the clearness index (k_t) (ratio of solar radiation to extraterrestrial solar radiation) [24, 26-27]. Recently, [28] have proposed the CIE (Commission Internationale de L'Éclairage) Standard Sky classification to specify the atmospheric characteristics and illumination levels of each of the established types in terms of energy and daylight. For this purpose, they proposed 15 CIE types of sky conditions.

Several methods are proposed in the literature for modeling of PAR and its derived ratios: a) the radiation transfer models which describe in detail the atmospheric processes [29-30] b) the artificial neural network [31] c) the estimation through satellite observations [32] and d) empirical models which differ in their complexity and the number of variables involved in the equations. The last category can be subdivided into three groups: i) Simple linear or multilinear models which are based on routinely measured parameters at meteorological stations, such as global radiation, sunshine duration and vapor pressure [33]; ii) power law models which are based mainly on clearness index, optical air mass and solar zenith angle [10,11,33] and iii) empirical models based on selected parameters which affect sky conditions such as the clearness of the sky (ϵ) and the brightness of skylight (Δ), global solar radiation, solar zenith angle optical air mass and dew point temperature [18,34-35].

Details about the measurements, quality control and modeling of solar radiation components at the study station are given by Pashiardis and Kalogirou [36]. Furthermore, (Pashiardis, et al. [37]) have studied the characteristics of PAR radiation at Larnaca, a coastal site of Cyprus. Jacovides et al. [17,20,31,38] have extensively studied various aspects of PAR radiation at the inland location of Athalassa, Cyprus, using different types of models.

The first objective of the study is to define the characteristics PAR values through a statistical analysis of hourly and daily values throughout the year and the second objective to implement various models and test them under the prevailing weather conditions at this station. Meanwhile, the levels of PAR were estimated under clear, partly cloudy and cloudy conditions. For this purpose, the clearness index (k_t) is used for classifying the sky conditions, i.e., cloudy sky ($k_t \leq 0.35$), partly cloudy ($0.35 < k_t < 0.65$) and clear sky ($k_t \geq 0.65$).

Materials and Methods

Hourly data of global horizontal irradiance (G) were obtained from the automatic weather station of Farmakas, a semi-mountainous location in Cyprus at the height of 833 m, covering the period 2016-2020. For the global radiation measurements, a CM-11 Kipp & Zonen pyranometer is used with an experimental error of approximately 2-3%. Its sensitivity is $8.21 \mu\text{V}/\text{W}/\text{m}^2$. For the sunshine duration data a Kipp & Zonen CSD3 sunshine duration sensor

is used. The sensor is facing south with a slope (β) of 35° from the horizontal plane. Sunshine duration is defined by WMO as the time during which the direct normal solar radiation exceeds the level of 120 W/m^2 . The sensor, at the same time, records the direct normal irradiance (B_n) in W/m^2 . The estimated value is less accurate than the value obtained by the pyrhiometer which is installed at a solar tracker system (Kipp & Zonen, personal communication). The photosynthetic active radiation is measured with a PAR-LITE Quantum Sensor of Kipp & Zonen and its sensitivity is $5.14 \mu\text{V}/\mu\text{mol/s m}^2$ with an experimental error of about 5%. This measurement rep-

resents the number of photons between 400 and 700 nm incident per square meter per second (Photosynthetic Photon Flux Density, PPF). The conversion factor of $4.57 \mu\text{mol/J}$ (or $\mu\text{mol/s /W}$) proposed by [13] is used to convert PPF into its energy alternative (i.e., PARE). All the sensors are factory calibrated. Additionally, the station is equipped with air temperature and relative humidity sensors which are installed at the screen level of 1.2 m above the surface. The station's coordinates are presented in Table 1. All radiation values were recorded at 1-min intervals, and hourly and daily values are derived from them through integration.

Table1: Station's coordinates and mean annual air temperature (T_a), Relative humidity (RH) and annual number of sunshine duration (S_d). 1= Shortest distance from coast in Km.

Station	Long. (E) (deg.)	Lat. (N) (deg.)	Elev. (m)	Distance ¹	Ta (°C)	RH (%)	S _d (hrs)
Farmakas	33.134	34.921	833	23	16.9	56	2555

The average air temperature in summer is about 27°C while during the winter is about 9°C . The maximum air temperature exceeds the value of 40°C on some days in the summer, while the lowest air temperature reaches -5°C in winter. The average annual rainfall is about 700 mm and occurs between October and May. The summer season is dry with almost clear sky conditions. Periodically, the island is under the effect of the Saharan Air Layer which is characterized by high content of mineral dust. Dust conditions are more frequent in spring and autumn, although they are also observed in some days in winter and summer. The prevailing wind direction is north-easterly during the day and south to south-easterly during the night. The average annual daily global radiation is 17.5 MJ/m^2 and the cumulative annual irradiation is about 6400 MJ/m^2 . The annual number of sunshine duration is about 2555 hours. About 145 days are considered as clear days. On the other hand, cloudy conditions are recorded in about 45 days.

Radiation Estimations and Quality Control Procedure

The analysis of this study has been limited to cases in which the solar elevation is higher than 5° due to the cosine response prob-

lem. The process of quality control for global and direct normal irradiances and the estimates of diffuse irradiances are described in detail by Pashiardis and Kalogirou [36]. The quality control of shortwave irradiances was based on physical possible, extremely rare and configurable limits, as proposed by BSRN group [39]. Generally, global irradiances (G) are lower than the extraterrestrial irradiances (G_0) in the same geographical location. Furthermore, the clearness index ($k_t = G/G_0$) should be larger than 0.03 but lower than 1. Similarly, PAR should be smaller than that at the top of the atmosphere for the same geographical coordinates and the daily ratio $f\text{FEC}_d$ (PPFD_d/G_0) must be in the range of 1.3-2.8 mol/MJ, otherwise the observation is considered as questionable [11]. Both criteria were satisfied as shown in Figure 1. G_0 and PARE_0 are calculated from the following equations. The irradiance falling on a plain at normal incidence at the top of the atmosphere (G_{0n}) can be estimated from [24]:

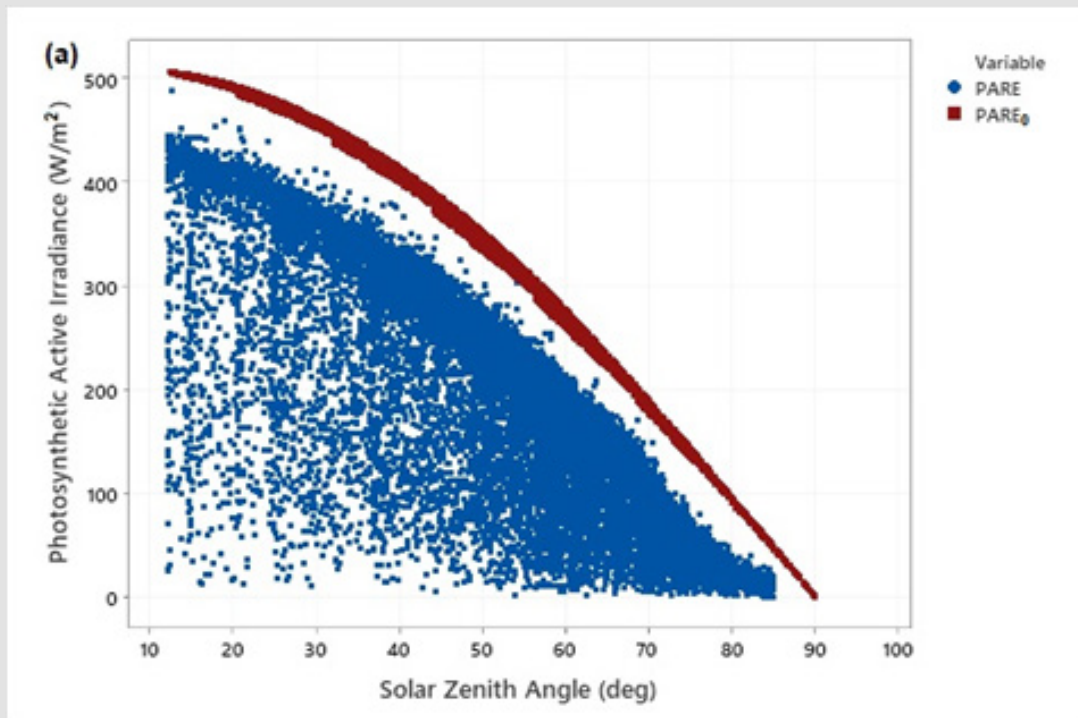


Figure 1a: Photosynthetic Active Irradiance at the ground level (PARE) and its value at the top of the atmosphere (PARE₀) as a function of the solar zenith angle.

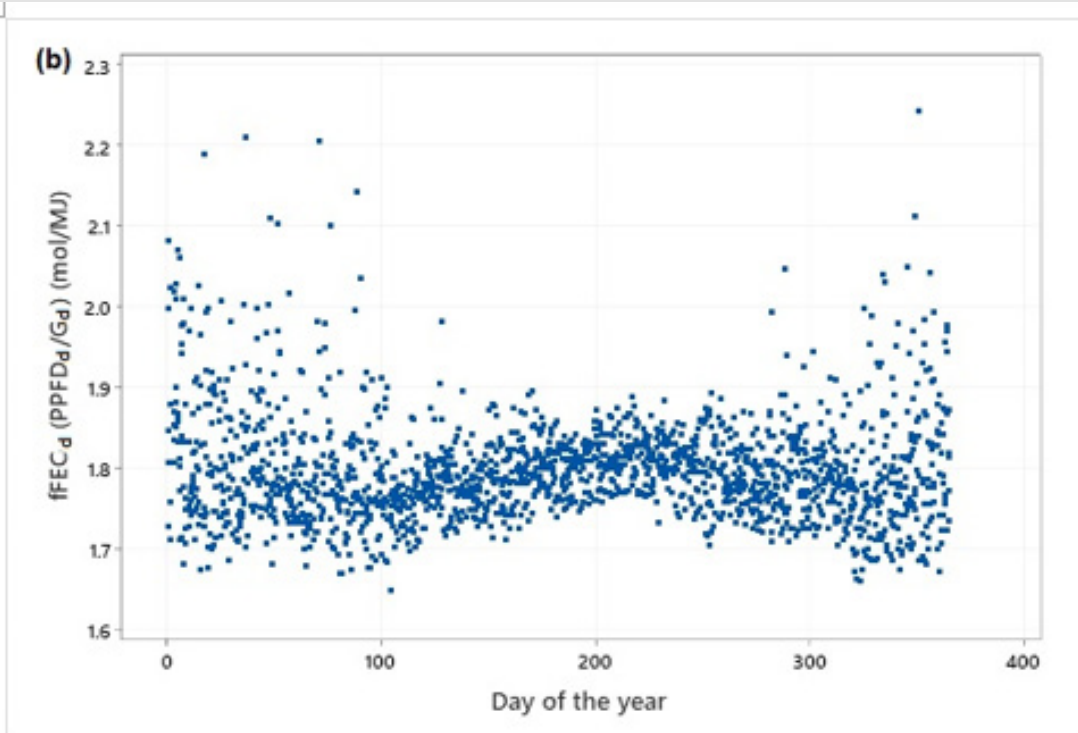


Figure 1b: Daily conversion efficiency (fFEC_d) at Farmakas during the period 2016-2020.

$$G_{0n} = G_{sc} * [1 + 0.033 * \cos(360 * d_n / 365)] \quad (W / m^2) \quad (1)$$

where G_{sc} is the solar constant for global radiation ($1367 \text{ W} / \text{m}^2$) and d_n is the day number of the year (1..365). The respective solar constant for PAR is $PAR_{sc} = 534.6 \text{ W} / \text{m}^2$ [25]. Then, the irradiance on a horizontal plain at the top of the atmosphere can be estimated by the following equation:

$$G_0 = G_{0n} * \cos \theta_z = G_{0n} * (\cos \phi * \cos \delta * \cos \omega + \sin \phi * \sin \delta) \quad (W / m^2) \quad (2)$$

where θ_z is solar zenith angle, ϕ is the latitude of the location, δ is the solar declination and ω is the hour angle. The solar declination and hour angles are estimated by the following equations:

$$\delta = 23.45 * \sin[360 * (284 + d_n) / 365] \quad (3)$$

$$\omega = 180 * (AST - 12) / 12 \quad (4)$$

where AST is the apparent solar time for the given day in hours. The local time (t) is converted to solar time (AST) using the following equation:

$$AST = t - 4(\lambda_{st} - \lambda) + Et - c \quad (5)$$

where c is the correction for summer time ($c=1$ for summer and $c=0$ for winter), is the reference longitude of the time zone which is positive to the east of Greenwich and for Cyprus is 30° , λ is the longitude of the location and Et is the equation of time in minutes which can be estimated from the following equations:

$$E_t = 9.87 * \sin 2A - 7.53 * \cos A - 1.5 * \sin A \quad (6)$$

$$A = 360 * (d_n - 81) / 365 \quad (7)$$

Then, the daily total global irradiation on a horizontal plain at the top of the atmosphere (G_{0d}) is given by:

$$G_{0d} = (24 * 3.6 / \pi) * G_{0n} * [(\cos \phi * \cos \delta * \sin \omega_s + (\pi * \omega_s / 180) * \sin \phi * \sin \delta)] \quad (kJ / m^2) \quad (8)$$

where ω_s is the sunset hour angle and is given by:

$$\omega_s = \cos^{-1}(-\tan \phi * \tan \delta) \quad (9)$$

The daily sums of global and PAR are obtained from the hourly values. The quality control process of global and PAR radiation was also extended to their daily values through various range tests. Figure 2 shows that the daily values of global and PAR radiation are within the specified limits. As stated earlier PAR is expressed in terms of either Photosynthetic Photon Flux Density (PPFD) in $\mu\text{mol} / \text{s} / \text{m}^2$ or in terms of Photosynthetic Active Irradiance (PAR) in W / m^2 which is more suitable for energy balance studies. From these terms the following indices can be derived: a) the fractional energy of PARE to global solar radiation (fPAR), b) the fraction of photon flux to energy conversion (fFEC, $\mu\text{mol} / \text{J}$ or mol / MJ), i.e., the ratio of PPFD to global radiation and c) the clearness index of PARE, i.e., the ratio of PARE to the extraterrestrial one ($PARE_0$). The above ratios including the clearness index take the following form:

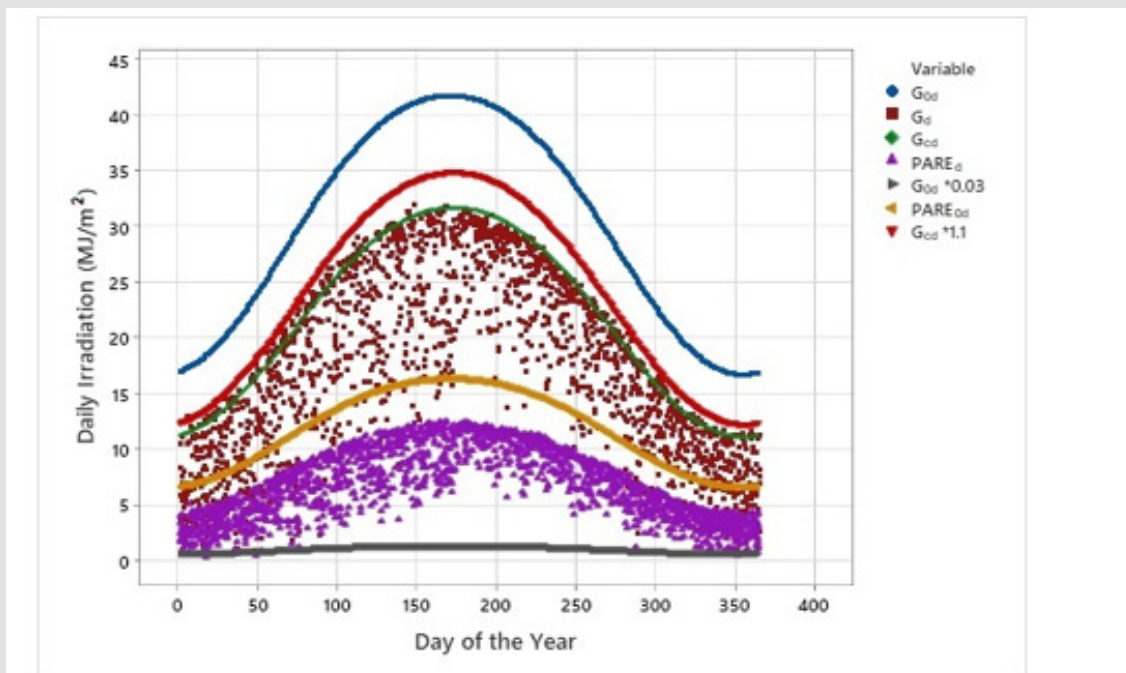


Figure 2: Range tests of daily irradiation values of global and PARE radiation (MJ / m^2).

$$fPAR = PARE / G \quad (10)$$

$$fFEC = PPFd / G \quad (11)$$

$$k_{PAR} = PARE / PARE_0 \quad (12)$$

$$k_t = G / G_0 \quad (13)$$

The above ratios can be obtained from both the hourly and daily values. The capital letters and subscripts represent the daily values, while the small letters represent the hourly values. The clearness index (k_t) is used for classifying the sky conditions: cloudy sky ($k_t \leq 0.35$), partly cloudy ($0.35 < k_t < 0.65$) and clear sky ($k_t \geq 0.65$) [11].

Psychrometric Estimations

The actual water vapor pressure (e_a) was estimated by the following equation:

$$e_a = e_s * RH / 100 \quad (14)$$

where RH is the relative humidity and e_s is the saturation vapor pressure estimated by Tetens [40] formula (Eq. 15) or by Eq. 16, provided by Murray [41] for temperatures below 0 °C in kilopascal:

$$e_s = 0.6108 * \exp\left(\frac{17.27 * T_a}{T_a + 237.3}\right) \quad (15)$$

$$e_s = 0.6108 * \exp\left(\frac{21.875 * T_a}{T_a + 265.5}\right) \quad (16)$$

where T_a is the air temperature in degrees Celcius. Vapor pressure deficit (VPD) and dew point temperature (T_d) were calculated from Eqs. 17 and 18:

$$VPD = e_s - e_a \quad (17)$$

$$T_d = \frac{116.9 + 237.3 * \ln(e_a)}{16.78 - \ln(e_a)} \quad (18)$$

Time Series

The time series plots of the daily global irradiation and PARE in MJ/m², as well as the daily PPFd in mol/m² and the sunshine duration in hrs/d are shown in Figure 3a. The highest values are recorded in the summer and the lowest in winter. The highest daily recorded global radiation is 31.9 MJ/m², while the highest daily PARE is 12.5 MJ/m². On the other hand, the highest daily value of PPFd is 57 mol/m² and the highest sunshine duration is 11.7 hrs/d. The daily variation of air temperature (T_a , °C), relative humidity (RH, %), actual vapor pressure (e_a , hPa) and clearness index (K_t) are shown in Figure 3b.

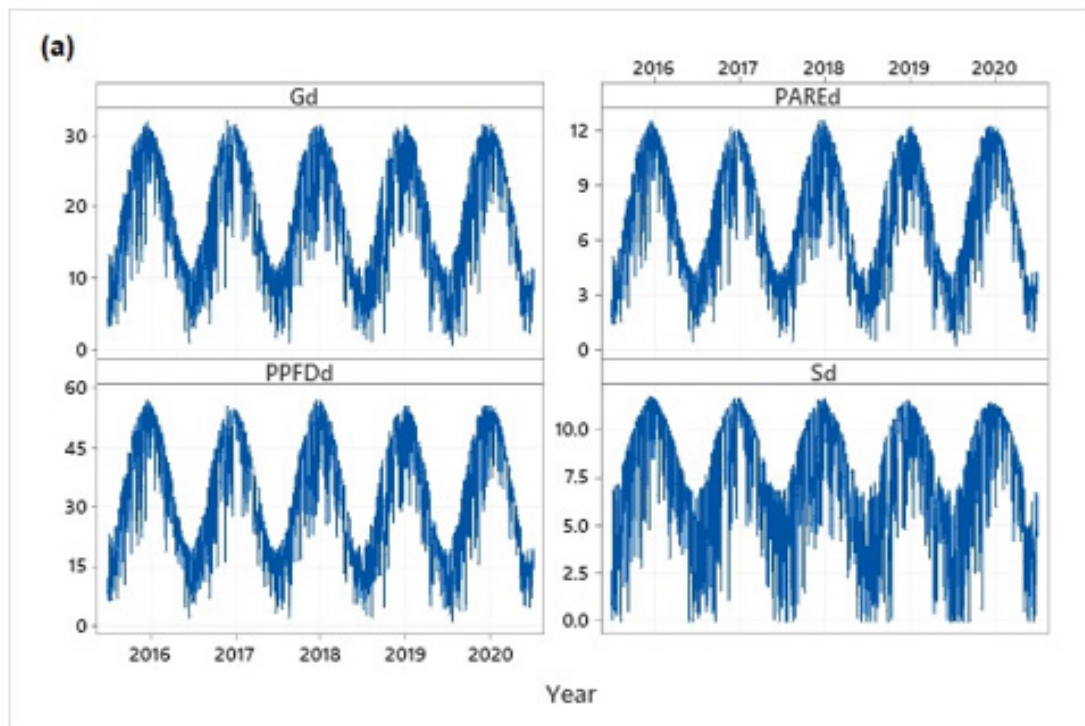


Figure 3a: Time series plots of daily global and PARE radiation in MJ/m², PPFd in mol/m² and sunshine duration in hrs/d.

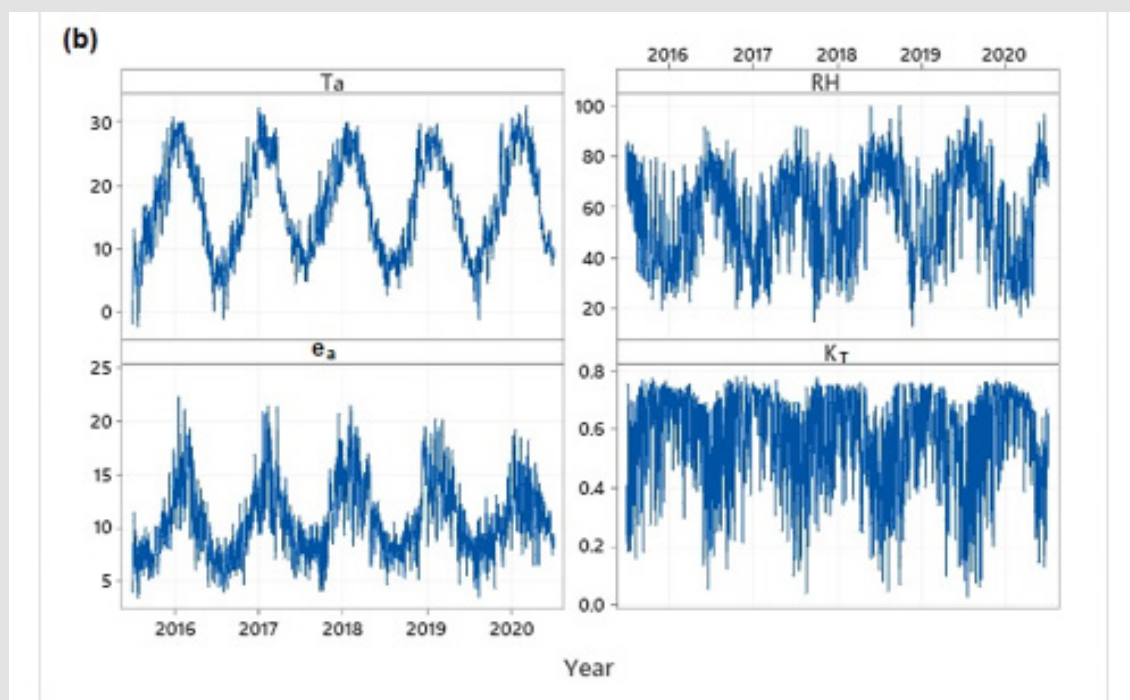


Figure 3b: Time series plots of daily values of air temperature (T_a , °C), relative humidity (RH, %), actual vapor pressure (e_a , hPa), and clearness index (K_T).

Results and Discussion

Hourly Values

Seasonal Variability of The Measured and Derived Variables: The monthly means and their standard deviations of the hourly measured and calculated variables are presented in Table 2a. The annual pattern of G and PAR fluctuations presents similar variability. As it can be seen, PARE range between 90 and 225 W/m^2 , while global irradiances range between 215 and 550 W/m^2 . The mean annual PPF is 776 $\mu mol/s/m^2$ with a seasonal variation between 410 $\mu mol/s/m^2$ in winter to 1025 $\mu mol/s/m^2$ in summer. The lowest mean temperatures occur in January and the highest in July ranging from 6.5 °C to 27.2 °C. In contrast, relative humidity ranges between 40% in July to 75% in January. The fraction of PARE to global ($fPAR$) is relatively constant throughout the year with an annual mean value of 0.412. The monthly means of $fFEC$ range from 1.816 $\mu mol/J$ in April to 1.914 $\mu mol/J$ in December with an annual average of 1.881 $\mu mol/J$. The clearness indices of global (k_g) and PAR (k_{PAR}) are comparable, with k_g ranging from 0.370 to 0.595, while k_{PAR} is fluctuating from 0.386 to 0.614. Both air and dew point temperatures (T_a and T_d) as well as the vapor pressure

parameters exhibit similar patterns with radiation, i.e., higher values in summer and lower values in winter. Based on hourly values, clear skies dominated the sky conditions (40%), followed by cloudy skies (35%) and then partly cloudy skies (25%) (Table 2b).

Diurnal Variations of Monthly Mean and Maximum Hourly Values: In Figure 4, monthly mean hourly (MMH) values of global and PAR in energy units (PARE, W/m^2) and in flux density units (PPFD $\mu mol/s/m^2$) are shown for Farmakas by means of isoline diagrams. These graphs show representative values of irradiances for each hour of every month of the year. July is the month with the maximum values of both radiation components. At noon, MMH of global irradiance is greater than 700 W/m^2 , and the PARE irradiance is greater than 380 W/m^2 . The highest mean hourly of global irradiance in July at local noon is 940 W/m^2 and the respective value of PPF is 1780 $\mu mol/s/m^2$ (Figures 4d & Figures 4e, respectively). Table 3 presents the maximum hourly values of global and PAR irradiances and the maximum hourly of PPF fluxes. As it can be seen, the measured maximum hourly global irradiance is 1161 W/m^2 , while PARE is 488 W/m^2 both obtained in July. The highest recorded PPF value is 2232 $\mu mol/s/m^2$.

Table 2a: Monthly means and standard deviations of hourly values of air temperature (T_a , °C), relative humidity (RH, %), global irradiance (G , W/m²), Photosynthetic Photon Flux Density (PPFD, $\mu\text{mol/s/m}^2$), Photosynthetic Active irradiance (PARE, W/m²), clearness index of global radiation (k_t), clearness index of PAR (k_{PAR}), fraction of PARE to global irradiance (fPAR) and the fraction of photon flux to energy conversion (fFEC) in $\mu\text{mol/J}$.

Mth	Ta (°C)		RH (%)		G (W/m ²)		PPFD ($\mu\text{mol/s/m}^2$)		PARE (W/m ²)		kt (G/G0)		kpar (PARE/PARE0)		fPAR (PARE/G)		fFEC (PPFD/G)	
	Mn	Std	Mn	Std	Mn	Std	Mn	Std	Mn	Std	Mm	Std	Mn	Std	Mn	Std	Mn	Std
1	6.5	3.47	75	13.2	216	188.2	411	319.8	90	70.0	0.371	0.230	0.386	0.214	0.418	0.052	1.911	0.234
2	8.5	4.35	69	18.0	298	233.6	551	395.9	121	86.6	0.432	0.246	0.441	0.228	0.415	0.050	1.891	0.214
3	11.2	4.43	60	19.9	380	287.4	739	478.2	162	104.6	0.488	0.248	0.512	0.224	0.409	0.054	1.863	0.228
4	15.1	5.43	52	21.9	464	316.1	858	540.2	188	118.2	0.535	0.238	0.541	0.217	0.398	0.041	1.816	0.188
5	19.8	6.11	48	20.7	479	328.5	907	575.3	199	125.9	0.536	0.233	0.550	0.217	0.402	0.049	1.839	0.216
6	23.6	5.51	48	19.9	513	329.6	951	600.5	208	131.4	0.560	0.233	0.570	0.223	0.406	0.065	1.875	0.271
7	27.2	5.41	39	17.7	548	338.8	1024	617.5	224	135.1	0.595	0.227	0.612	0.211	0.410	0.066	1.892	0.283
8	26.3	5.36	45	19.9	499	328.0	1003	554.0	219	121.2	0.565	0.232	0.614	0.192	0.424	0.074	1.917	0.303
9	23.6	5.75	48	21.1	454	299.6	864	512.7	189	112.2	0.551	0.236	0.575	0.211	0.415	0.059	1.883	0.240
10	18.6	5.01	57	21.4	364	258.7	684	437.3	150	95.7	0.502	0.243	0.521	0.217	0.416	0.059	1.893	0.249
11	12.8	4.08	68	18.4	266	218.2	548	349.5	120	76.5	0.442	0.240	0.474	0.217	0.420	0.067	1.900	0.258
12	9.0	3.66	74	15.2	214	181.8	420	300.2	92	65.7	0.391	0.232	0.412	0.212	0.422	0.065	1.914	0.254
Year	16.9	8.59	57	22.5	405	308.5	776	540.8	170	118.3	0.506	0.246	0.526	0.226	0.412	0.060	1.881	0.250

Table 2b: Monthly means and standard deviations of dew point temperature (T_d , °C), saturation vapor pressure (e_s , k_{pa}), actual vapor pressure (e_a , k_{pa}), and vapor pressure deficit (VPD, kPa), along with percentages of cloudy, partly cloudy and clear sky conditions according to the classification of the clearness index (k_t).

Month	T_d (°C)		e_s (k_{pa})		e_a (k_{pa})		VPD (k_{pa})		Percentage of data (%)		
	Mean	StDev	Mean	StDev	Mean	StDev	Mean	StDev	$k_t \geq 0.35$	$0.35 < k_t < 0.65$	$k_t \geq 0.65$
1	2.3	3.67	1.00	0.236	0.74	0.179	0.25	0.176	56.1	24.7	19.2
2	2.6	3.73	1.16	0.362	0.76	0.187	0.4	0.35	47.7	25.8	27.4
3	2.7	4.18	1.39	0.431	0.78	0.218	0.61	0.46	35.8	28.6	35.7
4	3.8	4.38	1.83	0.686	0.84	0.24	0.99	0.733	29.0	27.4	43.6
5	6.8	3.95	2.5	1.042	1.03	0.268	1.46	1.099	29.0	27.1	43.9
6	10.5	4.29	3.12	1.093	1.33	0.371	2.78	1.15	24.0	25.4	50.7
7	10.4	4.8	3.86	1.285	1.35	0.428	3.51	1.355	18.7	22.4	59
8	11.7	5.22	3.67	1.239	1.48	0.424	2.19	1.341	23.3	23.1	53.7
9	10.2	5.09	3.15	1.197	1.33	0.430	1.81	1.281	29.3	17.3	53.4
10	8.5	4.68	2.27	0.789	1.17	0.341	1.1	0.863	32.2	27.5	40.3
11	6.5	3.96	1.54	0.446	1.00	0.243	0.54	0.45	46.7	22.2	31.2
12	4.2	3.6	1.18	0.305	0.85	0.198	0.33	0.269	50.7	27.2	22.1
Year	6.7	5.49	2.23	1.301	1.06	0.408	1.17	1.17	35.1	24.9	40.0

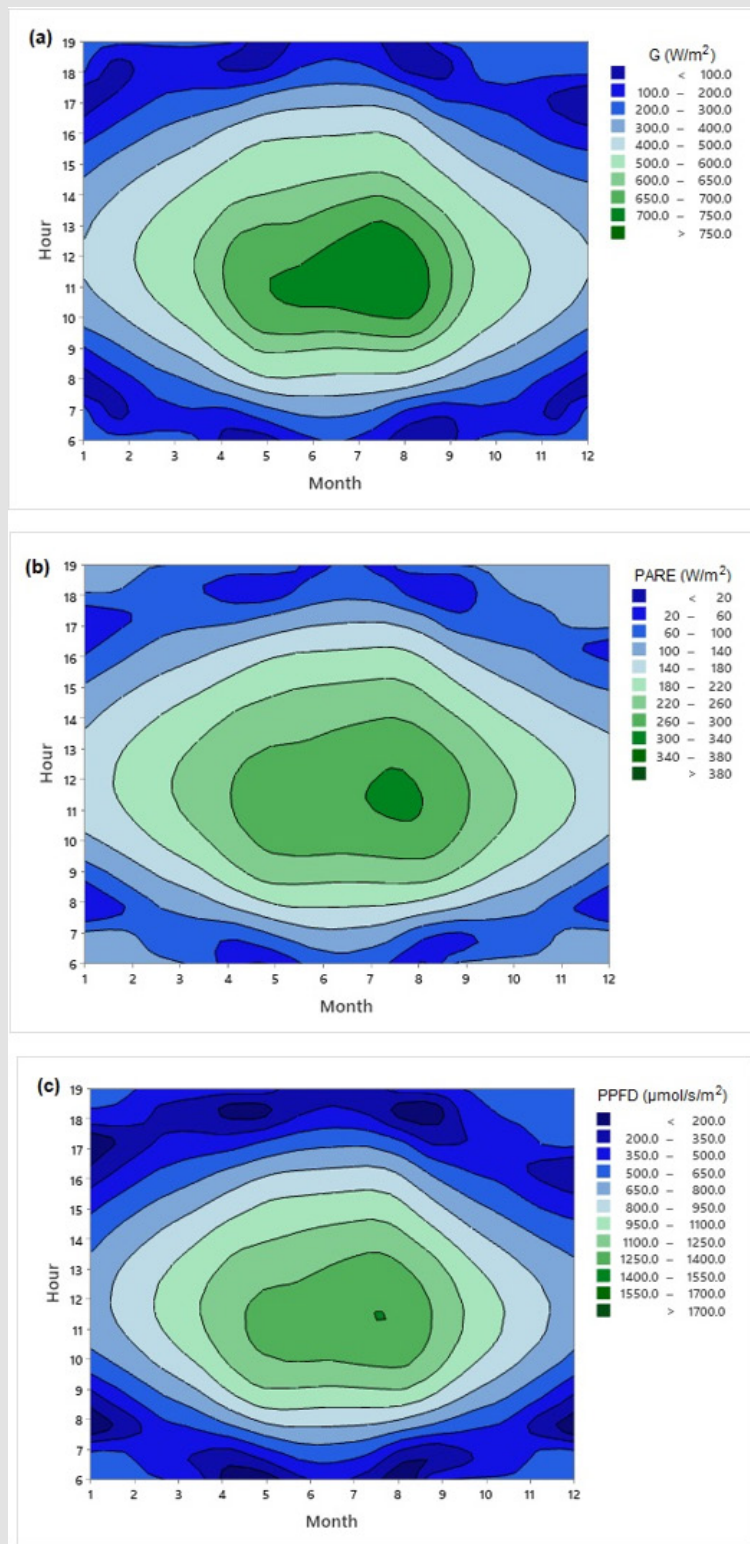


Figure 4: Isoline diagrams of monthly mean hourly of

- a) global (W/m²),
- b) PARE irradiance values (W/m²) and
- c) PPFD flux density values (µmol/s/m²).

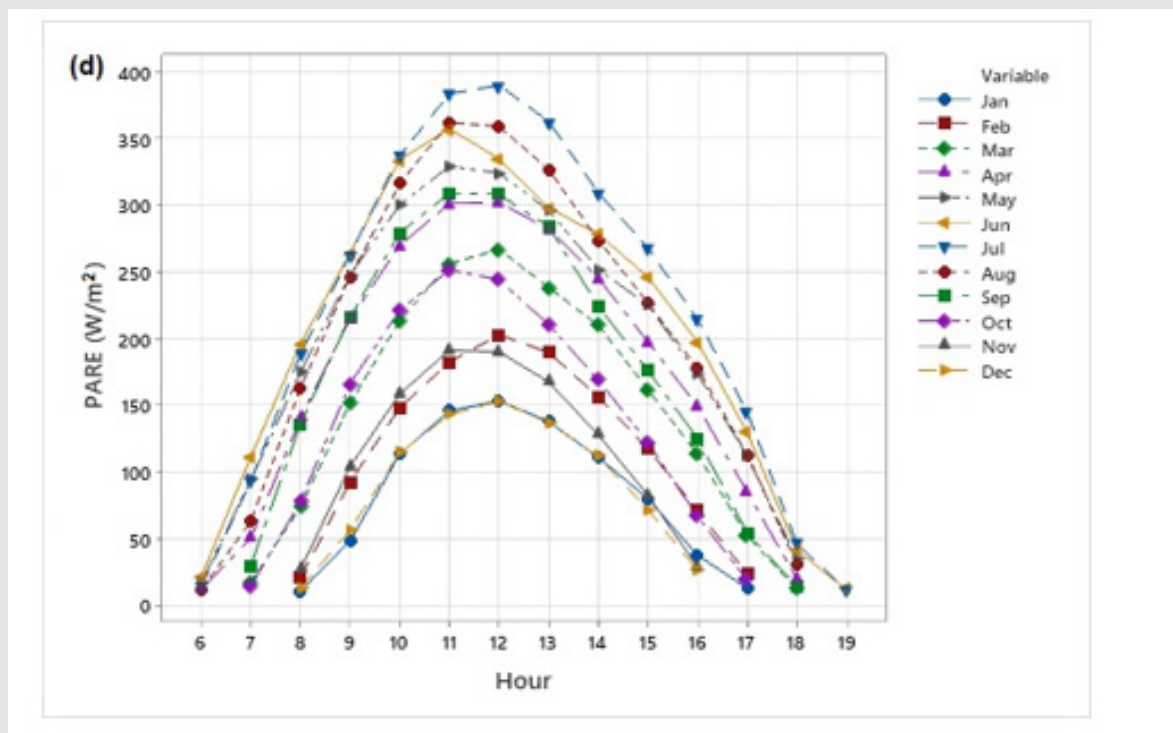


Figure 4d: Diurnal evolution of hourly values of Photosynthetic Active Irradiance (PARE, W/m²).

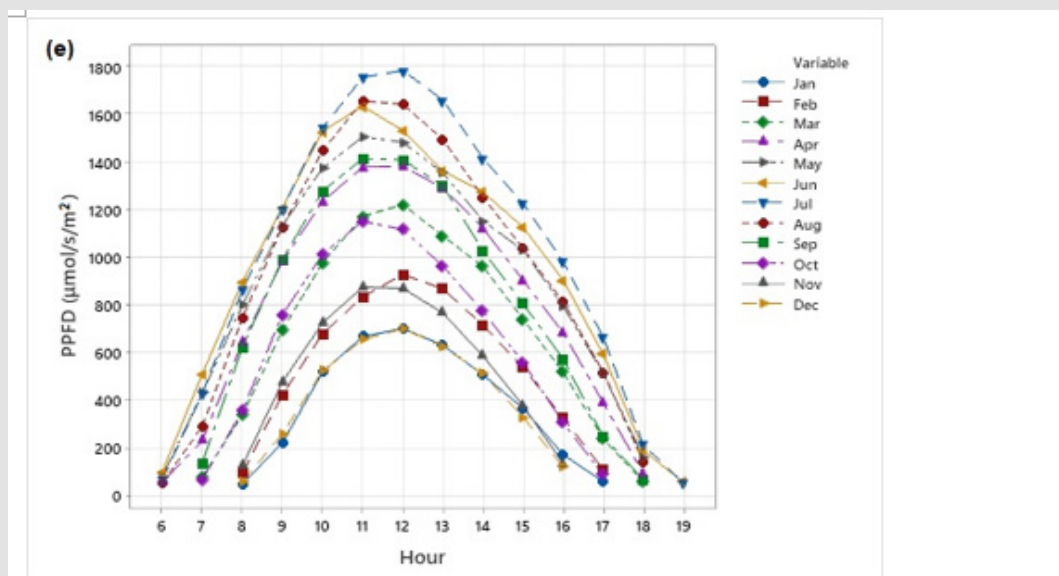


Figure 4e: Diurnal evolution of hourly values of Photosynthetic Photon Flux Density (PPFD, µmol/s/m²).

Table 3: Maximum hourly values of global and PARE irradiances and the maximum hourly PPFD fluxes.

Maximum of G (W/m²)													
Hour	Jan	Feb	Mar	Apr	May	Jun	Jul	Aug	Sep	Oct	Nov	Dec	All
05:00 - 06:00				15	31	32	20	13					32
06:00 - 07:00			37	90	123	128	117	86	53	24			128
07:00 - 08:00	22	52	142	184	220	221	207	181	158	131	58	29	221

08:00-09:00	94	166	224	270	295	317	283	268	239	209	161	100	317
09:00-10:00	176	237	300	359	372	395	378	343	314	280	221	179	395
10:00-11:00	230	299	361	410	440	452	440	412	391	347	270	211	452
11:00-12:00	278	325	384	430	458	445	488	427	393	340	301	248	488
12:00-13:00	304	346	376	412	430	444	454	413	382	349	281	226	454
13:00-14:00	254	285	326	370	402	407	407	376	337	275	211	208	407
14:00-15:00	186	237	264	305	323	351	330	320	272	218	153	149	351
15:00-16:00	72	155	204	215	252	265	254	233	192	146	62	51	265
16:00-17:00	22	67	97	132	169	181	173	150	102	39			181
17:00-18:00			23	38	59	63	67	54	26				67
18:00-19:00						16	15						16
All	304	346	384	430	458	452	488	427	393	349	301	248	488

Maximum of PARE (W/m ²)													
Hour	Jan	Feb	Mar	Apr	May	Jun	Jul	Aug	Sep	Oct	Nov	Dec	All
05:00 - 06:00				15	31	32	20	13					32
06:00 - 07:00			37	90	123	128	117	86	53	24			128
07:00 - 08:00	22	52	142	184	220	221	207	181	158	131	58	29	221
08:00-09:00	94	166	224	270	295	317	283	268	239	209	161	100	317
09:00-10:00	176	237	300	359	372	395	378	343	314	280	221	179	395
10:00-11:00	230	299	361	410	440	452	440	412	391	347	270	211	452
11:00-12:00	278	325	384	430	458	445	488	427	393	340	301	248	488
12:00-13:00	304	346	376	412	430	444	454	413	382	349	281	226	454
13:00-14:00	254	285	326	370	402	407	407	376	337	275	211	208	407
14:00-15:00	186	237	264	305	323	351	330	320	272	218	153	149	351
15:00-16:00	72	155	204	215	252	265	254	233	192	146	62	51	265
16:00-17:00	22	67	97	132	169	181	173	150	102	39			181
17:00-18:00			23	38	59	63	67	54	26				67
18:00-19:00						16	15						16
All	304	346	384	430	458	452	488	427	393	349	301	248	488

Maximum of PPFD (μmol/s/m ²)													
Hour	Jan	Feb	Mar	Apr	May	Jun	Jul	Aug	Sep	Oct	Nov	Dec	All
05:00- 06:00				69	143	146	91	59					146
06:00- 07:00			169	411	560	584	533	392	244	109			584
07:00- 08:00	99	239	647	839	1007	1008	948	828	722	600	264	131	1008
08:00- 09:00	430	758	1023	1236	1346	1447	1294	1227	1091	953	735	459	1447
09:00- 10:00	806	1084	1371	1642	1701	1805	1726	1566	1437	1281	1012	820	1805
10:00- 11:00	1049	1368	1650	1872	2009	2065	2009	1885	1785	1584	1233	966	2065
11:00- 12:00	1270	1486	1753	1966	2095	2032	2232	1953	1794	1553	1377	1133	2232
12:00-13:00	1387	1581	1720	1883	1963	2027	2074	1888	1747	1597	1283	1032	2074
13:00- 14:00	1159	1302	1488	1693	1837	1858	1861	1719	1539	1256	962	951	1861
14:00- 15:00	850	1083	1205	1394	1475	1602	1510	1462	1245	998	699	683	1602
15:00- 16:00	330	708	933	984	1152	1212	1163	1067	877	665	283	235	1212
16:00- 17:00	100	308	441	604	773	825	790	687	464	177			825
17:00- 18:00			106	175	270	290	305	246	121				305
18:00- 19:00						75	68						75
All	1387	1581	1753	1966	2095	2065	2232	1953	1794	1597	1377	1133	2232

Variability Of Global and PAR Irradiances and The Relevant Indices: The variability of the measured irradiances is demonstrated with the graph of boxplots for each month of the year. The boxplot presents the median and the Interquartile Range (IQR) as well as the outliers (asterisks) of each variable (Figure 5a). The smooth line represents the mean values of irradiances for each month of the year. As it can be seen no outliers are observed for the hourly global and PARE irradiances. The PARE irradiance on clear days is about 50 to 100 W/m² higher than that under any other weather conditions. The highest variability of all variables is observed in the summer months as it is indicated by the length of the boxes. The variability of clearness indices are shown in Figure 5b. The similarities between the two clearness indices are evident. fPAR and

fFEC are relatively constant throughout the year, with an annual mean value of 0.412 and 1.881 μmol/J, respectively. The daily evolution of hourly values of fFEC is shown in Figure 5c. As it can be seen the ratio fFEC is higher in the morning and afternoon hours, while it is more stable during midday. Higher ratios are found under conditions of high cloud cover or higher water content in the atmosphere, a result that supports the findings of various authors [18,20,26]. PAR fraction reaches its highest value during sunrise or sunset and decreases to its lowest values around 08.00 in the morning and around 17.00 in the afternoon. During the rest of the day it is relatively constant throughout the year (Figure 5c). This diurnal rhythm is mainly due to the diurnal cycle of water vapor. Similar results have been reported by Hu et al.[21] in different areas of China.

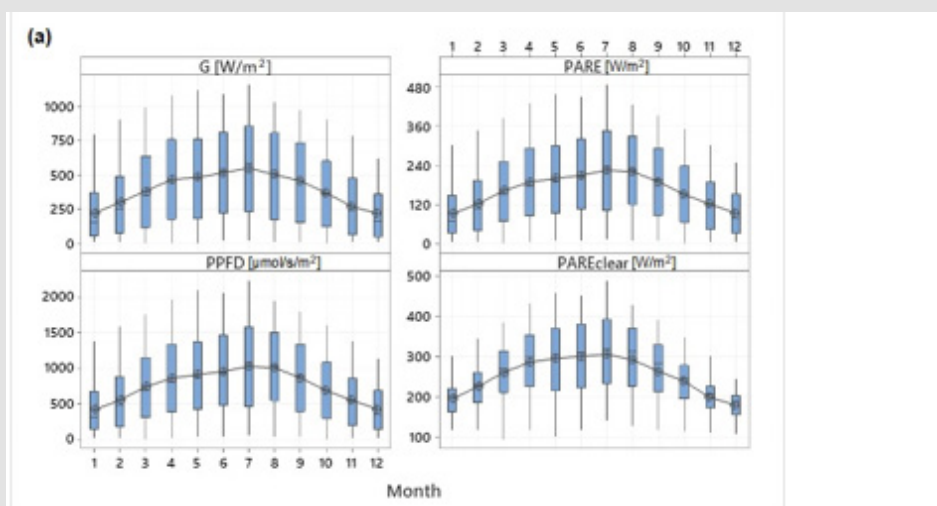


Figure 5a: Boxplots of hourly irradiances in W/m² and PPFD fluxes in μmol/s/m² of each month of the year.

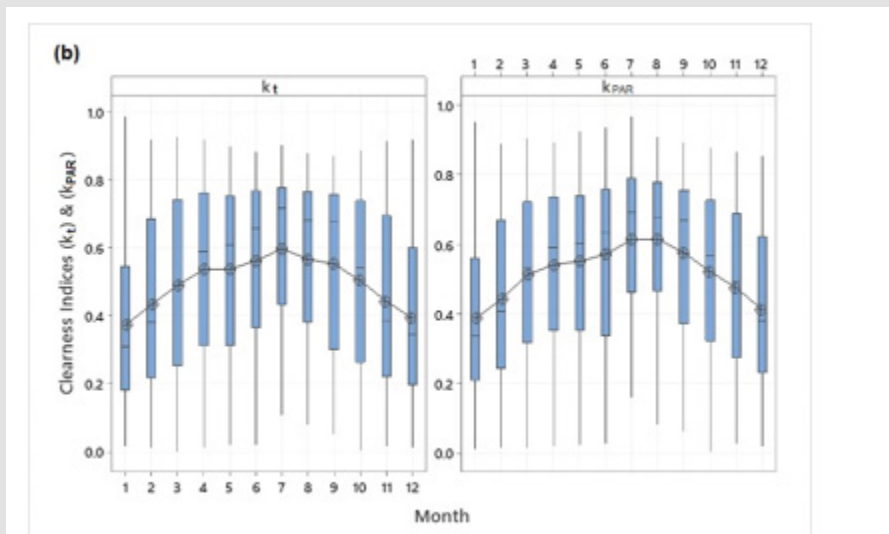


Figure 5b: Boxplots of clearness indices of global (k_t) and PAR radiation (k_{PAR}) of each month of the year.

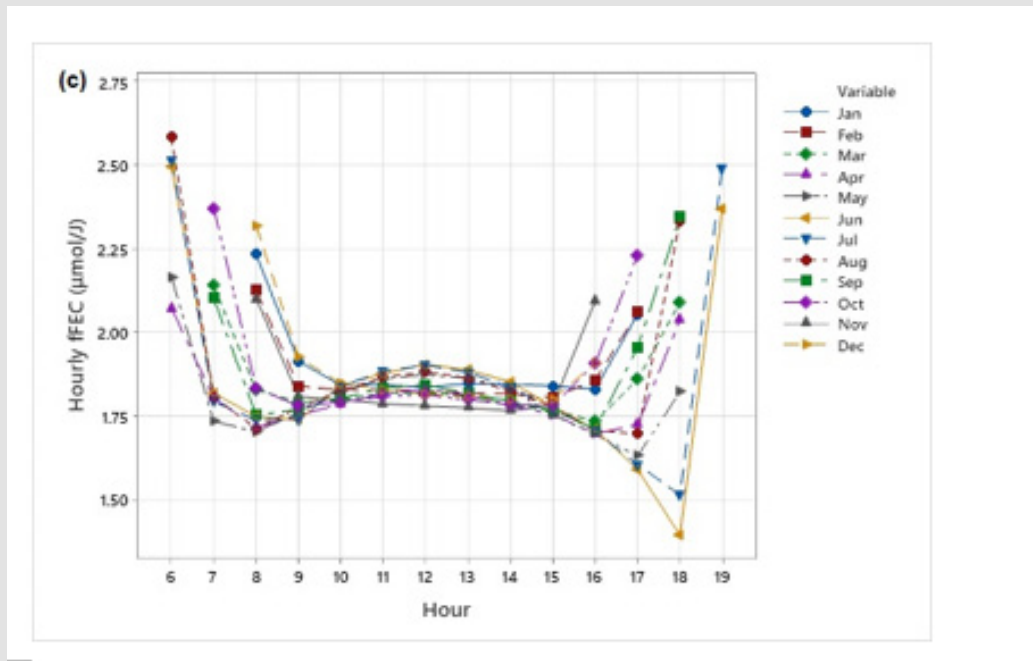


Figure 5c: Daily evolution of fFEC (µmol/l) at Farmakas for each month of the year.

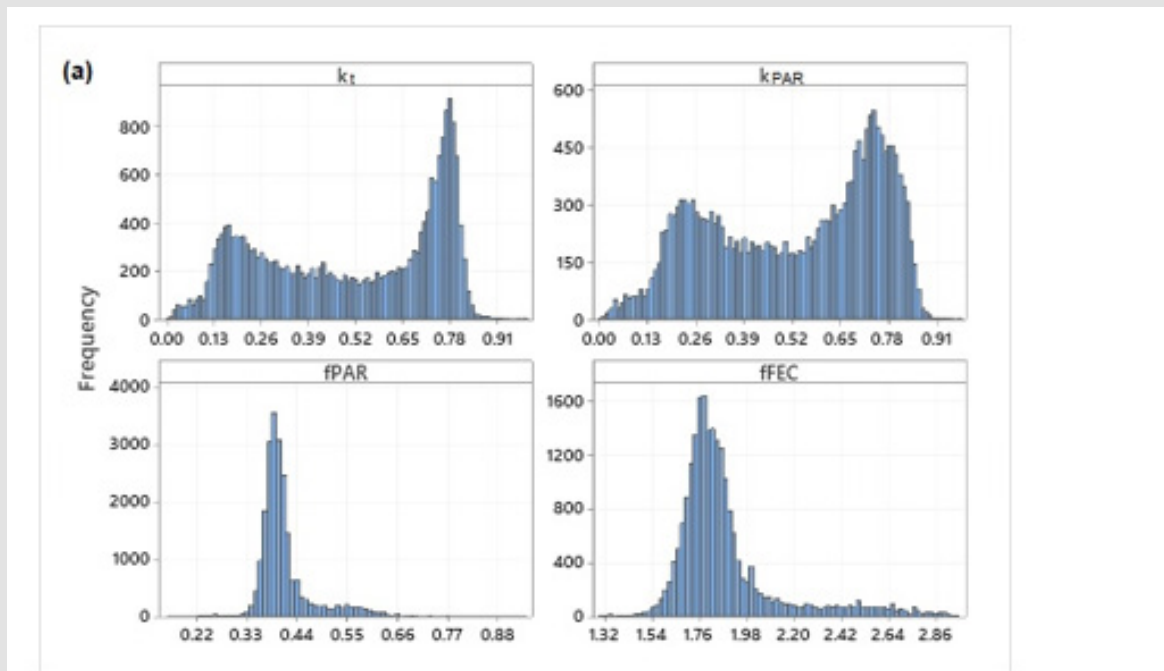


Figure 6a: Frequency distributions of hourly values of k_t , k_{PAR} , $fPAR$ and $fFEC$ variables at Farmakas during the study period.

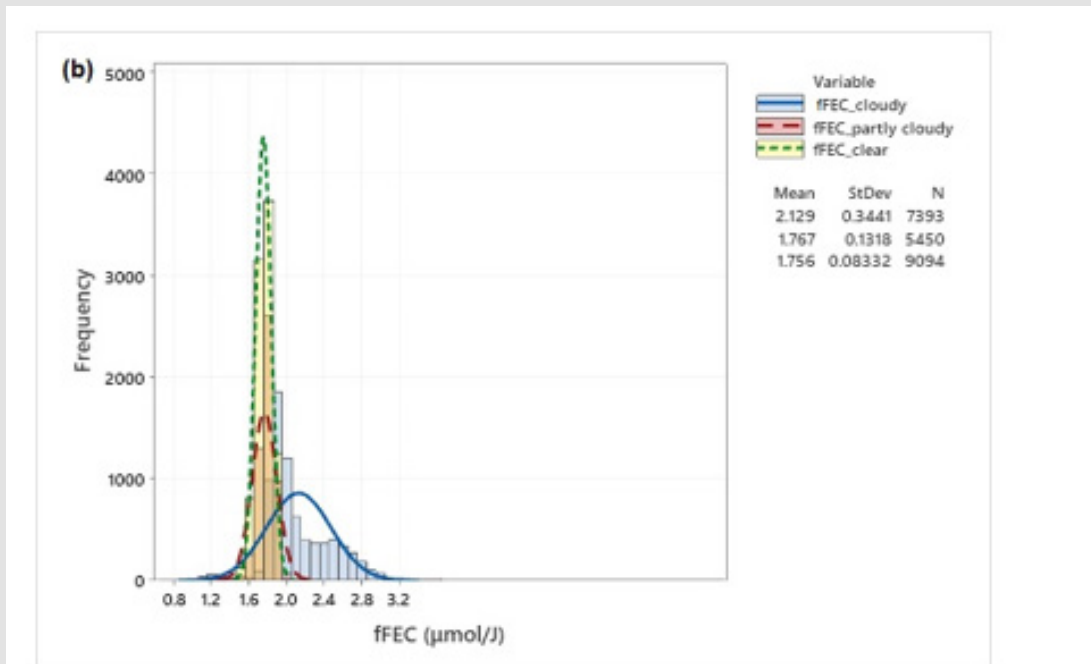


Figure 6b: Frequencies of hourly fFEC for the three different classes of sky conditions.

It is known that clouds, gases and aerosols may interrupt the transmission of solar irradiance through the atmosphere; clearness index k_t is a general indicator of the absorption and scattering effects and it is used for characterizing sky conditions [11,24]. k_t was also used for investigating the relationship between PARE and G under various sky conditions in each month. Figure 6a shows the frequency distribution of hourly k_t , k_{PAR} , fPAR and fFEC variables at Farmakas during the study period. The pattern of frequency distributions of both clearness indices (k_t and k_{PAR}) is almost similar. Regarding the frequency distribution of fFEC, it can be seen from Figure 6a that a larger predominance (71.7%) is observed for the interval of $1.7 \mu\text{mol/J} < \text{fFEC} < 2.0 \mu\text{mol/J}$, with the largest frequencies (of about 90%) occurring when hourly fFEC was smaller than $2.1 \mu\text{mol/J}$. Most of the data (78.2%) were recorded at e_a values greater than 0.8 kPa, whereas cases of very low water vapor pressure ($e_a < 0.4$ kPa) are very rare (0.5%). The variability of PAR fraction is mainly controlled by the selective scattering of aerosol particles and absorption of water vapor. The annual average of fFEC is $1.756 \mu\text{mol/J}$, $1.763 \mu\text{mol/J}$ and $2.129 \mu\text{mol/J}$ for clear, partly cloudy and cloudy days, respectively (Figure 6b). The cloudy day's ratio is therefore about 20% higher than that for clear days and partly cloudy days.

Hourly Relationships: Linear relationships with strong correlations were established between hourly PARE terms and the respective global irradiances:

$$PARE = -0.543 + 0.392 * G \left(\frac{W}{m^2} \right) \quad R^2 = 0.994 \quad (19)$$

$$PPFD = -4665 + 1.792 * G \left(\mu\text{mol}/s/m^2 \right) \quad R^2 = 0.994 \quad (20)$$

The slopes without the intercepts are 0.391 and 1.789, respectively. The slopes between PARE and G during the winter season vary between 0.381 and 0.384, in spring and autumn they range between 0.385 and 0.391, and in summer they range between 0.392 and 0.398. The monthly slopes of PPFD and G range between 1.742 and $1.760 \mu\text{mol/J}$ during the winter months and they are higher during the rest of the year ranging from 1.765 to $1.820 \mu\text{mol/J}$. The clearness indices also show high correlation:

$$k_{PAR} = 0.033 + 0.935 * k_t \quad R^2 = 0.98 \quad (21)$$

The effect of the solar position, global irradiance, clearness index and actual vapor pressure on the ratio of fFEC ($\mu\text{mol/J}$) is shown in Figure 7. We can observe that this ratio varies between 1.3 and $2.8 \mu\text{mol/J}$ with a mean value of $1.847 \pm 0.2 \mu\text{mol/J}$, and with slightly more scatter for longer path lengths (Figure 7a). Thus, there is no clear dependence of the ratio on solar position, even though the values tend to be higher for solar position close to zenith. Alados et al. [18] and Foyo-Moreno et al. [42] Found similar results. A similar picture is observed for the ratio with global irradiance (Figure 7b). Thus, for high values of G, the ratio tends to a value close to its mean value, whereas for low values of G the ratio has high dispersion. A similar picture is obtained with the clearness index (k_t), i.e., at cloudy conditions ($k_t < 0.35$) the ratio shows higher values, while at clear conditions the ratio shows less dispersion with values around its mean value (Figure 7c). Finally, there is no relationship between fFEC and actual vapor pressure (Figure 7d). Similar picture is obtained with dew point temperature (T_d) (not shown here).

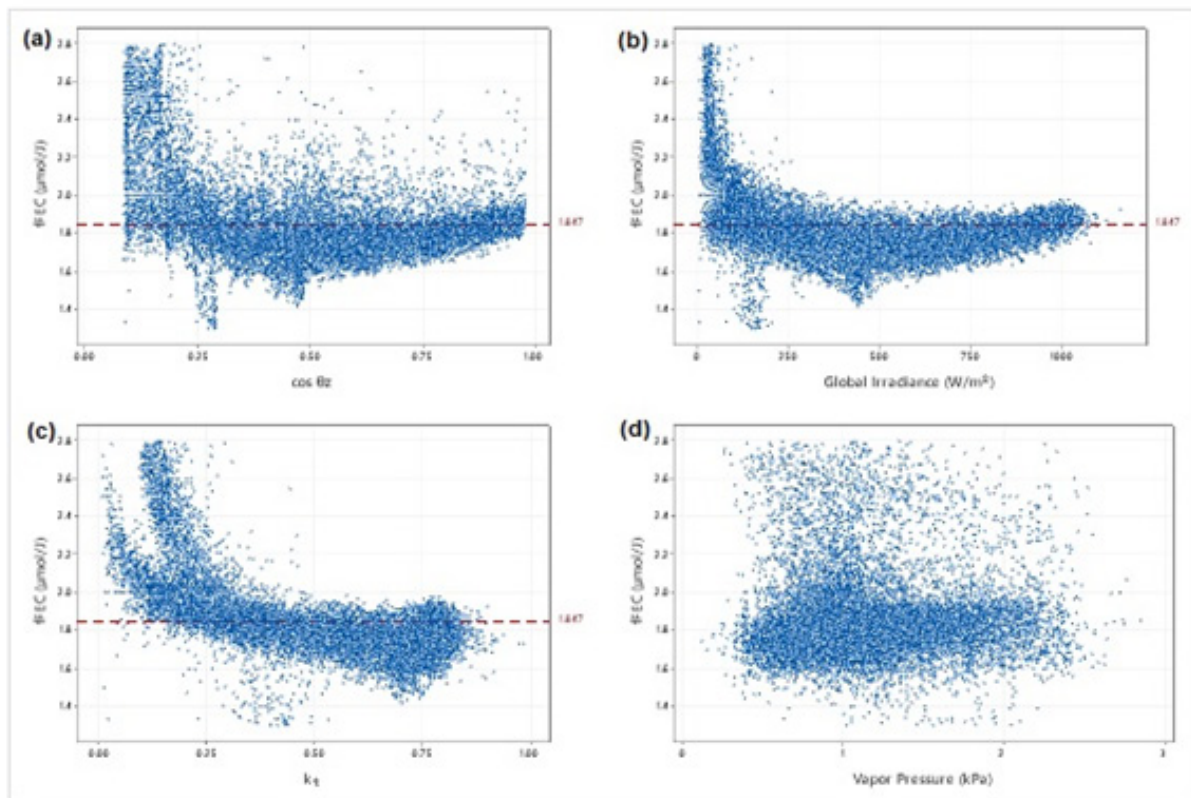


Figure 7: Ratio of photosynthetic photon flux density to global irradiance (fFEC) versus a) cosine of solar zenith angle ($\cos\theta_z$), b) global irradiance (G), c) clearness index (k_t) and d) water vapor pressure (e_a).

Model Development and Validation: In the literature, there are a lot of empirical or semi-empirical models for estimating PAR using global radiation, air temperature, sunshine hours and other meteorological variables [43]. However, these models are applicable only under the local conditions and extensions of these models to other sites are restricted. Furthermore, some models are only effective in clear skies conditions [22, 44-45]. Six different models varying in their complexity will be tested. The model accuracy will be evaluated by the scatterplots of the linear relationship between the measured and estimated values. Various statistical indicators, such as the mean bias error (MBE), the root mean square error (RMSE), the relative error (RE) and the coefficient of determination (R^2) will be used to assess the accuracy of the models. The estimation of the above indicators are given by the following equations:

$$MBE = \frac{1}{n} \sum_{i=1}^n (E_i - M_i) \tag{22}$$

$$RMSE = \sqrt{\frac{1}{n} \sum_{i=1}^n (E_i - M_i)^2} \tag{23}$$

$$RE = \frac{1}{n} \sum_{i=1}^n [(|E_i - M_i|)M_i] * 100 \tag{24}$$

where, E_i is the estimated value, M_i is the measured one and n is the number of observations. The coefficients of the models are estimated using data from the period 2016-2019 (training data set) and their validation is based on the data of the year 2020 (validation data set).

As stated earlier six models different in their complexity will be used to estimate the PAR component. The simplest one is the linear relationship between PPFD and global irradiance (G) (Eq. 25) or "model A":

$$PPED = \alpha * G \tag{25}$$

where α is the regression parameter (slope of the line).

Monthly PAR variations reflect those of global radiation (G) (Figure 5). Monthly PAR variations are mainly controlled by seasonal variations of astronomical factors and by fluctuations of meteorological conditions (clouds, water vapor, aerosols, etc.) [17-18]. Numerous studies show that k_t can represent the effects of the

above factors on the transmission of solar radiation through the atmosphere. Thus, k_t is added to improve the accuracy of the estimate (Eq. 26) or "model B":

$$PPFD = \alpha * G + b * k_t + c \quad (26)$$

where α, b, c are regression coefficients.

The third model relates the PAR transmissivity (k_{PAR}) with the clearness index (k_t) and the relative optical air mass (m). The parameterization model has the following form (Eq. 27) or "model C":

$$k_{PAR} = \alpha * k_t^b * m^c \quad (27)$$

where, α, b, c are regression coefficients. The optical air mass can be calculated from the Kasten and Young [46] equation as:

$$m = (p / p_0) / (\sin a_s + 0.50572 * (a_s + 6.07995)^{-1.6364}) \quad (28)$$

$$(p / p_0) = \exp(-z / 8400) \quad (29)$$

where α_s is the solar elevation angle and z is the elevation of the station in m. Figure 8 shows the dependence of hourly PAR on optical air mass (m) under different sky conditions. It is clear that PAR generally decreased with increasing m and the maxima are recorded when sky conditions are clear. A smaller degree of dispersion is evident between PAR values under clear weather and m conditions. The estimation model for PPFDclear takes the following form:

$$PPFD_{clear} = 1721.4 * m^{-1.20} \quad (30)$$

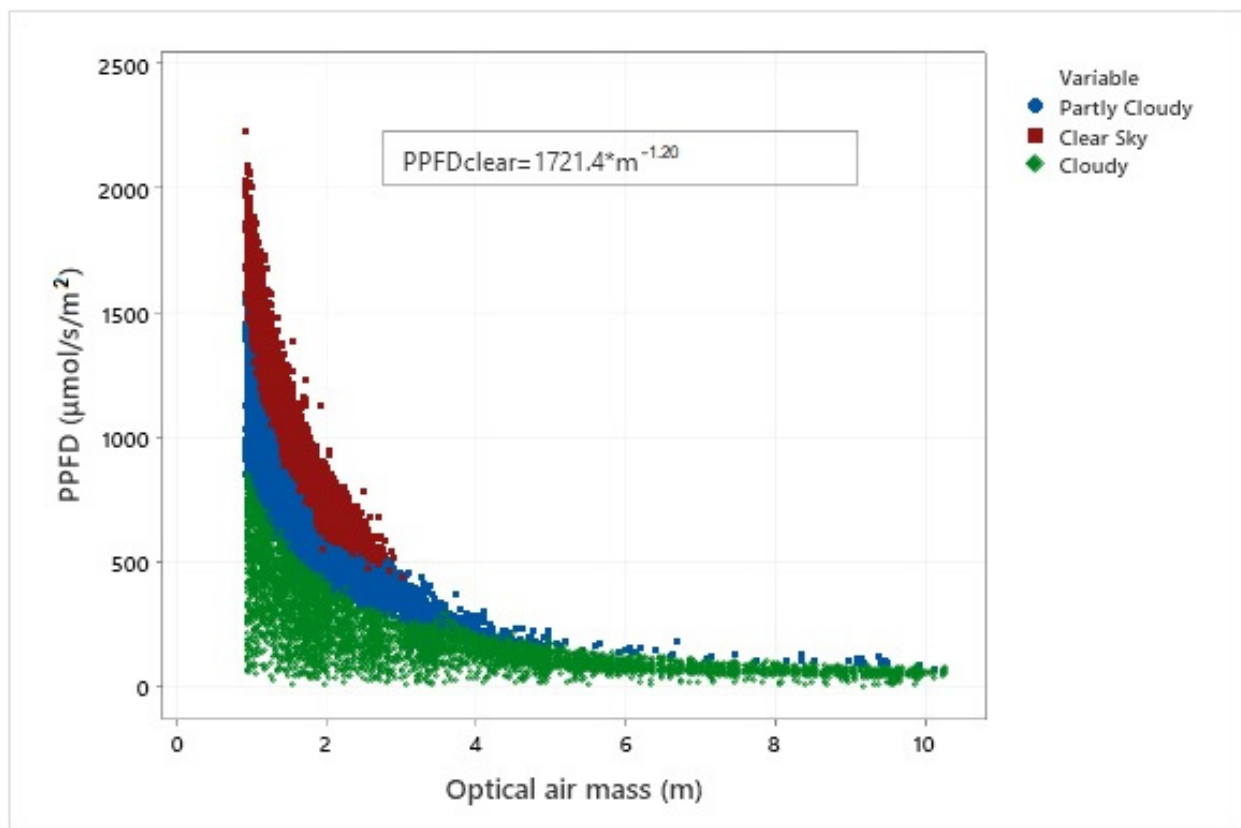


Figure 8: Dependence of hourly PPFD on optical air mass under different sky conditions at Farmakas.

The fourth model, "model D" is similar to the third one, but the optical air mass is replaced by the ratio PAR under clear skies to that at the top of the atmosphere (AF_{clear}). The $PPFD_{clear}$ under clear skies is estimated by Eq. (30). Therefore, the model takes the form [33]:

$$PPFD = (\alpha * AF_{clear}^b * k_t^c) * PPFD_0 \quad (31)$$

where $PPFD_0$ is the extraterrestrial PAR in units of $\mu\text{mol/s/m}^2$. The fifth model, "model E", relates PAR with k_t and the cosine of solar zenith angle (μ). Figure 9 depicts the dependence of PPFD on k_t and the cosine of solar zenith angle μ . PAR is increased exponentially with increasing μ for a constant k_t . The dependence of PPFD on μ is described with a power law equation. Therefore, PAR could be calculated for a narrow k_t range with the following equation [44]:

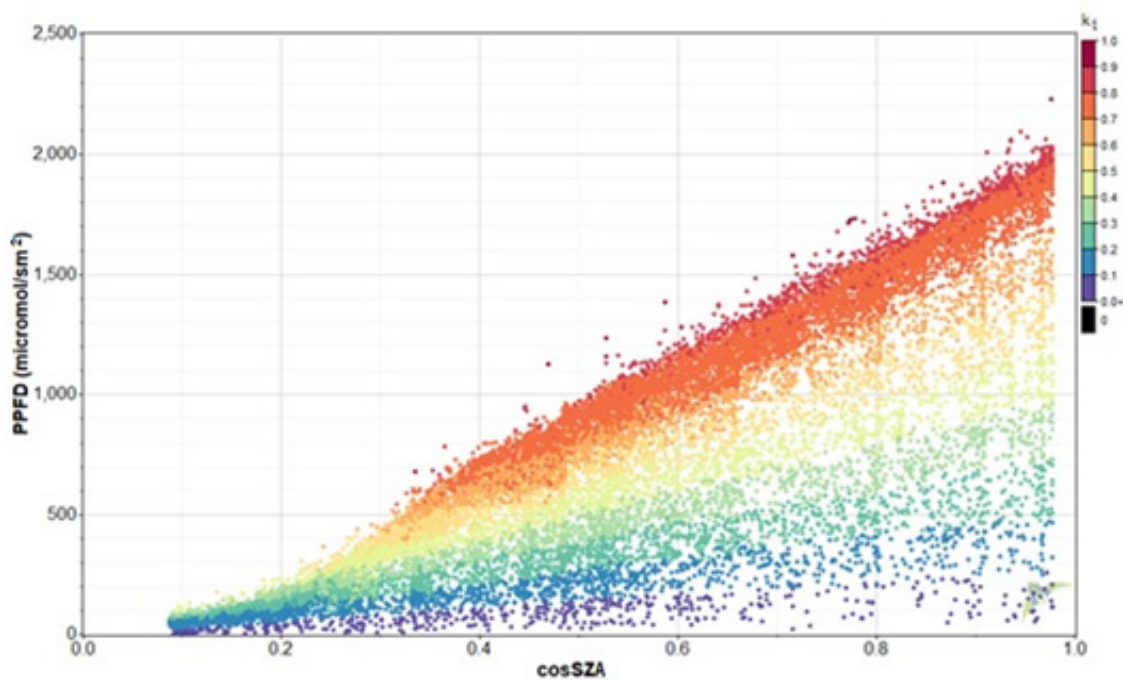


Figure 9: The relationship between PPFD with the clearness index (k_t) and the cosine of the solar zenith angle at Farmakas (different k_t values are represented by different colors).

$$PPFD = PPFD_x * \mu^\alpha \tag{32}$$

where $PPFD_x$ is the maximum PPFD per μ and α describes how PPFD changes with μ . $PPFD_x$ is expressed as a function of k_t . The estimation of the parameters of the Eq. (26) is done in two steps. Firstly, $PPFD_x$ is found by binning of k_t in increments of 0.02. Then, the dependence of $PPFD_x$ on k_t for the training data set (2016-2019) is described by a cubic equation:

$$PPFD_x = 63.77 + 2080 * k_t + 977 * k_t^2 - 742.7 * k_t^3 \quad R^2 = 0.998 \tag{33}$$

The relationship between PPFD and μ (through α) is investigated using a non-linear regression approach:

$$PPFD = PPFD_x * \mu^{1.09} \tag{34}$$

Almost similar values were obtained by Wang, et al. [11] in Inner Mongolia in China.

The sixth model (model F) was proposed by Foyo-Moreno, et al. [42] and is a simple empirical model which estimates PPFD through the expression:

$$PPFD = a * k_t * \cos \theta_z \tag{35}$$

Estimation of the Model's Parameters: As it is indicated in the previous section, the data set was split into the training set (2016-2019) and validation data set (2020). The estimated model parameters which are based on the training data set hourly measurements are shown in Table 4. As it can be seen, all models have high coefficient of determination (R^2). In all cases, the slopes (f) of the regression lines between the estimated values and the measured ones are close to 1. With the exception of model C all other models show relatively low values of the statistical indicators of MBE, RMSE and RE. Therefore, the simple model A which is based on only one parameter (global radiation) and the empirical multi-linear models B and F are essentially the best one (Figure 10).

Table 4: Estimation model parameters (α , b and c) using six different models based on the data set of the period 2016-2019 and the validation was based on the data set of the year 2020. The values e and f represent the intercept and the slope of linear regression between the estimated and measured PPDF variables. R^2 is the coefficient of determination. MBE and RMSE are in units of $\mu\text{mol/s/m}^2$.

Estimation Model	α	b	c	e	f	R^2	MBE	RMSE	RE (%)
Model A	1.787			7.8	0.98	0.995	-3.5	41.1	7.9
Model B	48.4	1.95	-228.3	6.6	0.99	0.997	-3.4	32.3	13.5
Model C	0.9	0.8	0.015	53.7	0.91	0.993	-8.9	67.2	10.6
Model 0	1.09	0.567	0.8	18.1	0.98	0.994	0.2	43.9	10.2
Model E	1.09			-14.7	1.01	0.996	-7.4	36.9	11.4
Model F	2403.3			-0.7	0.99	0.995	-5.9	41	10.2

Daily Values

Seasonal Variation of Daily Global and Photosynthetic Active Radiation:

Figure 3a shows the temporal evolution of daily irradiation components at Farmakas. Data reveal a common evolution shape with maxima in summer and minima in winter, due to the daily minimum solar zenith angle and day-length (astronomical factors) variation during the year. Large fluctuations are occurred in spring and autumn during the transition from cold to warm weather and vice versa. As stated earlier, the maximum of daily global solar horizontal irradiation is reached in June or July and it is almost 32 MJ/m^2 while the maximum daily PARE is 12.5 MJ/m^2 . Figure 3b shows also the temporal evolution of the rest meteorological parameters measured at this station. Daily air temperatures range mainly between -2 to $32 \text{ }^\circ\text{C}$ with an annual mean of about $17 \text{ }^\circ\text{C}$. Actual vapor pressure ranges between 3.5 to 22 hPa with an annual daily average of 10.6 hPa . The respective annual mean daily relative humidity is 57% .

Table 5 shows the mean daily values and their standard deviations of all the radiation components for each month of the year for the whole period of measurements. The variability of the daily values of the global and PAR radiation is also demonstrated

through the boxplots of each month of the year (Figure 11). The smooth curve represents the mean daily values of each month of the year. As indicated from the length of the boxplots, the spring season shows the greatest variability. Outliers are observed mainly in July. The monthly mean daily values of the global and PARE radiation components are lower than those obtained at Athalassa and Larnaca [37]. The mean daily global radiation ranges from 7.7 MJ/m^2 in December to 27.6 MJ/m^2 in July with an annual mean daily value of 17.5 MJ/m^2 . The respective mean daily PARE_d ranges from 3.0 MJ/m^2 in December to 10.9 MJ/m^2 in July with a mean annual value of 6.9 MJ/m^2 . The mean daily PARE_d ranges from 13.7 mol/m^2 in December to 49.8 mol/m^2 in July with a mean annual value of 31.4 mol/m^2 . The highest daily value of PPDF_d is 57.0 mol/m^2 . The frequency distribution of the above variables is presented in Figure 12a, while the cumulative density functions CDF are demonstrated in Figure 12b.

Figure 12a shows that the distribution of all variables is almost similar. Figure 12b indicates that in 75% of the year, the daily sums of global irradiation is less than 24.5 MJ/m^2 , less than 9.5 MJ/m^2 for PARE, less than 43.5 $13.7 \text{ mol/m}^2/\text{d}$ for PPDF and less than 10 hrs/d for sunshine duration.

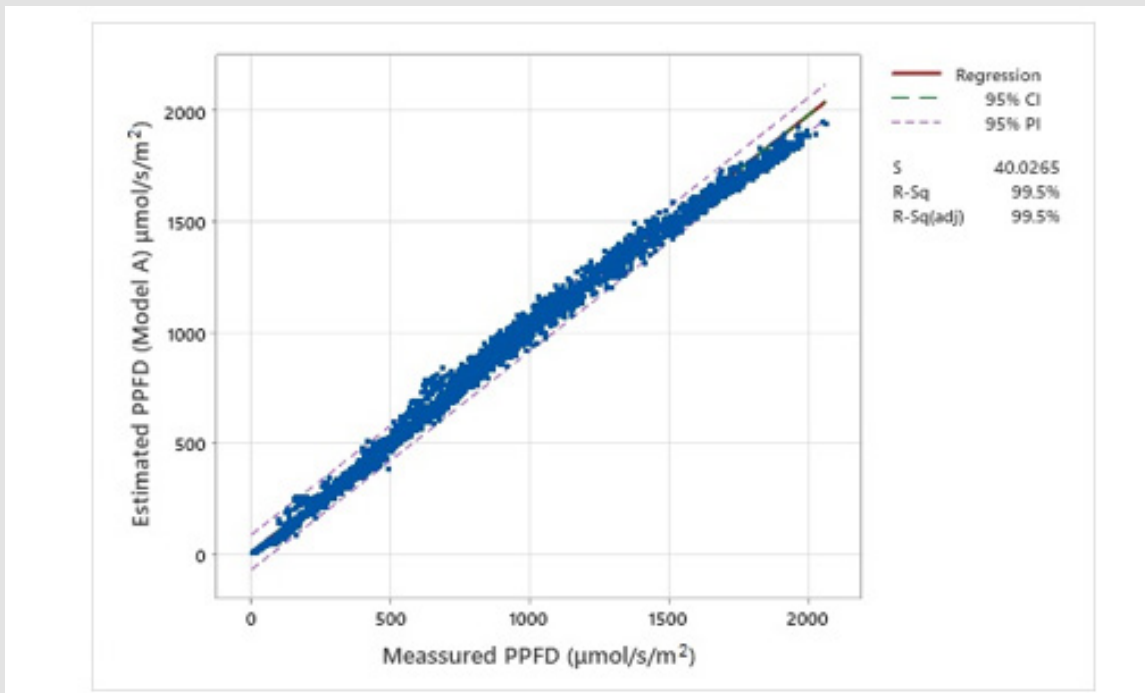


Figure 10: A comparison between estimated and measured PPFD in $\mu\text{mol/s/m}^2$ based on validation data set using model A.

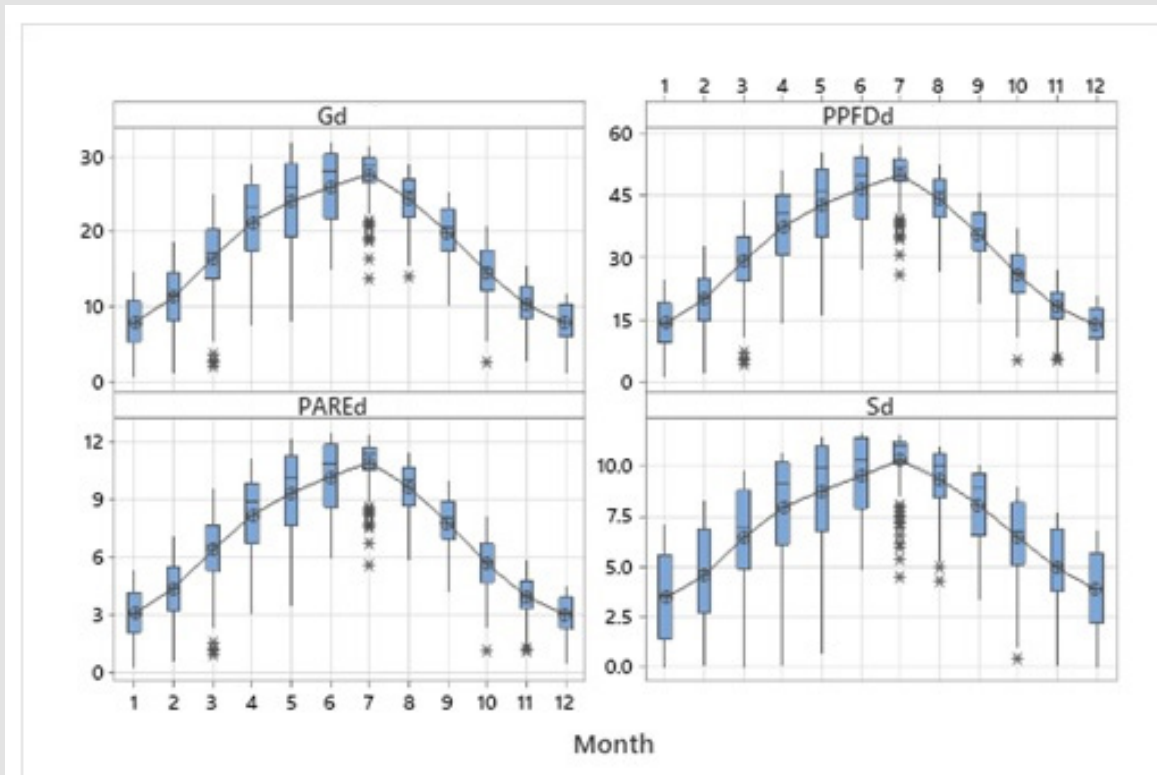


Figure 11: Boxplots of daily Global (G_d) and PARE_d in MJ/m^2 , daily PPFD_d in $\text{mol/m}^2/\text{d}$ and sunshine duration (S_d) in hrs/d for each month of the year. The smooth line represents the mean daily values of each month for each variable

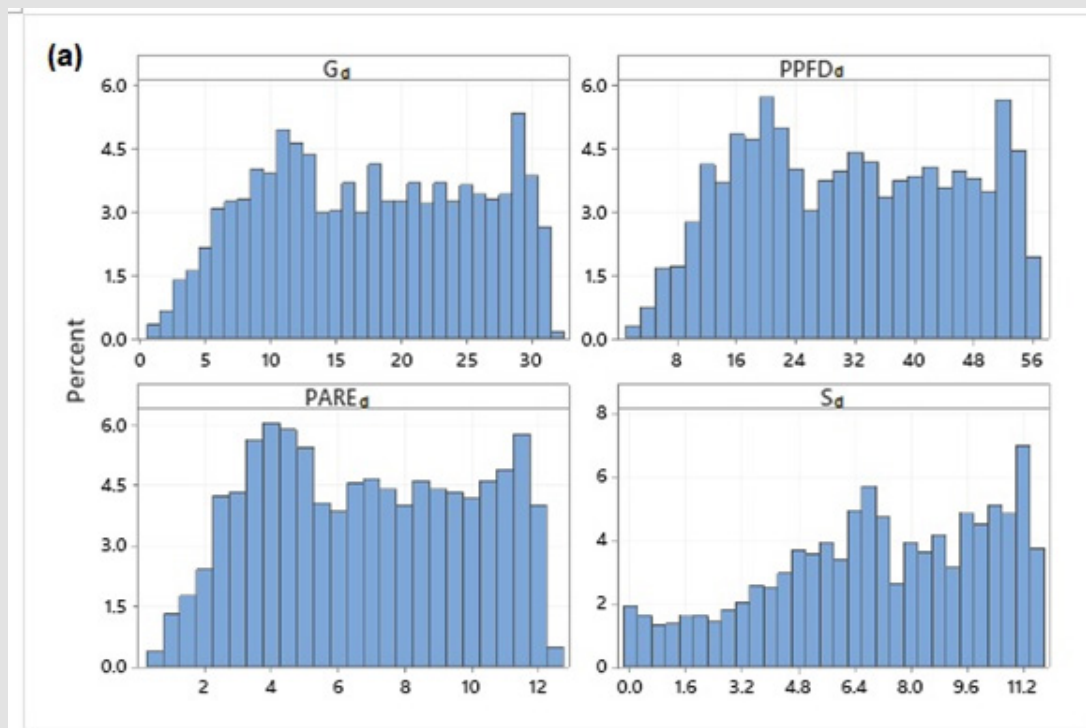


Figure 12a: Frequency distribution of daily values of global (G_d), $PARE_d$, $PPFD_d$ and sunshine duration (S_d) at Farmakas.

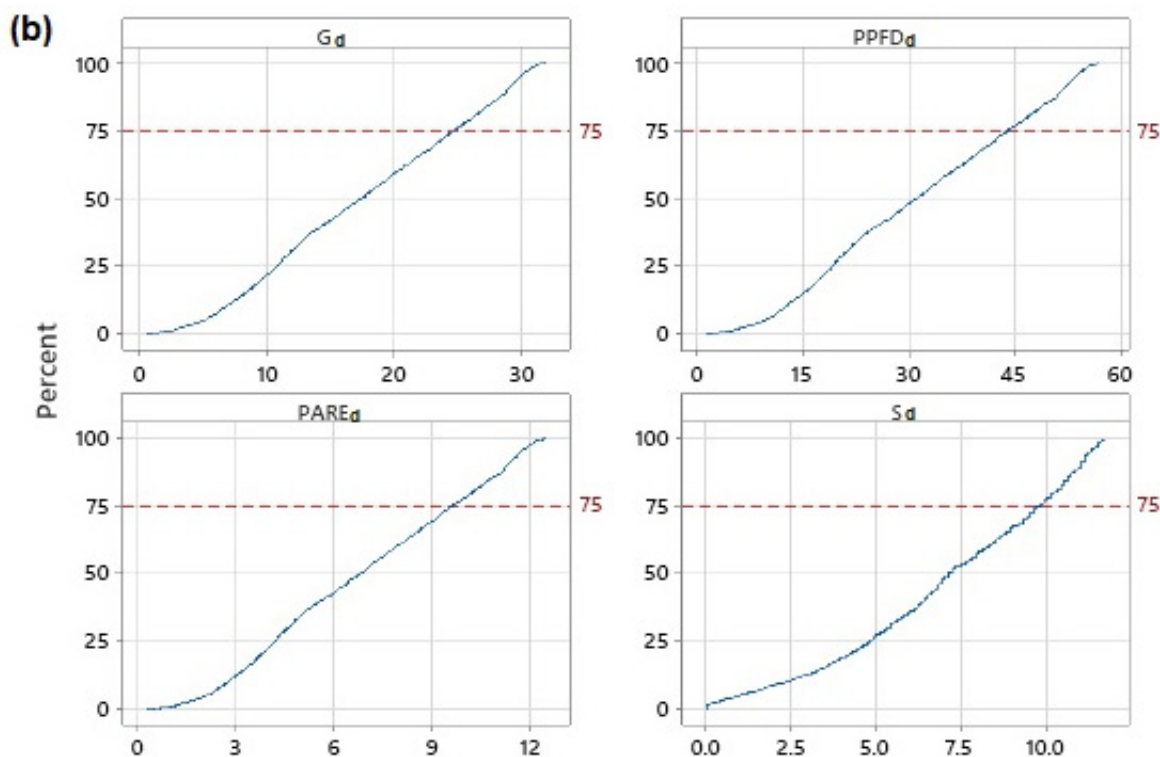


Figure 12b: Cumulative density function (CDF) of global(G_d), $PARE_d$, $PPFD_d$ and sunshine duration (S_d) at Farmakas

Table 5: Mean daily statistics of global, PARE components for each month of the year and for the whole period of measurements (MJ/m²) as well as monthly mean daily sunshine duration in hrs/d.

Month	N	G _d (MJ/m ² /d)				PARE _d (MJ/m ² /d)				PPFD _d (mol/m ² /d)				S _d (hrs/d)			
		Mean	StDev	Min	Max	Mean	StDev	Min	Max	Mean	StDev	Min	Max	Mean	StDev	Min	Max
1	155	7.8	3.28	0.5	14.5	3.1	1.19	0.3	5.4	14.0	5.42	1.2	24.5	3.4	2.30	0.0	7.1
2	140	11.1	4.11	1.0	18.8	4.4	1.50	0.5	7.2	19.9	6.87	2.1	32.7	4.6	2.47	0.0	8.3
3	155	16.4	5.19	1.9	24.9	6.3	1.89	0.9	9.5	29.0	8.63	4.1	43.5	6.4	2.77	0.0	9.8
4	150	21.2	5.80	7.3	28.9	8.2	2.12	3.0	11.1	37.3	9.66	13.8	50.9	7.9	2.75	0.1	10.7
5	155	23.9	5.75	7.9	31.9	9.3	2.16	3.4	12.1	42.6	9.89	15.7	55.4	8.8	2.55	0.6	11.5
6	150	25.8	4.89	14.7	31.7	10.2	1.88	5.9	12.5	46.4	8.57	26.8	57.0	9.5	2.15	4.8	11.7
7	155	27.6	3.29	13.7	31.4	10.9	1.23	5.6	12.4	49.8	5.60	25.6	56.5	10.3	1.44	4.5	11.6
8	155	24.3	3.48	13.9	29.1	9.6	1.33	5.8	11.4	43.9	6.06	26.3	52.3	9.4	1.56	4.3	11.0
9	150	19.8	3.79	10.1	25.3	7.8	1.40	4.1	9.9	35.4	6.38	18.8	45.5	8.1	1.84	3.3	10.1
10	155	14.4	3.70	2.5	20.6	5.6	1.35	1.1	8.1	25.7	6.18	5.1	36.9	6.5	1.96	0.4	9.0
11	150	10.1	2.95	2.4	15.5	3.9	1.07	1.1	5.9	17.9	4.92	4.9	27.1	4.9	2.07	0.0	7.8
12	155	7.7	2.74	0.9	11.8	3.0	0.98	0.5	4.5	13.7	4.46	2.1	20.6	3.9	2.12	0.0	6.8
Year	1825	17.5	8.10	0.5	31.9	6.9	3.15	0.3	12.5	31.4	14.37	1.2	57.0	7.0	3.16	0.0	11.7

Daily Clearness Index and Relative Sunshine Duration: The clearness index (K_r), for a particular time interval, is defined as the ratio of the global radiation to the extraterrestrial radiation. It is an objective measure of the influence of cloud cover on the solar radiation flux. As it was indicated earlier three different classes are defined according to the values of the daily clearness index. The variation of the daily clearness index throughout the year is shown in Figure 13. It is clear that in summer months there are no cloudy days. The monthly statistics based on the daily clearness index values for Farmakas are reported in Table 6. Also listed in the table is the number of days according to the above classification for each of the month of the year. The annual average of K_r is 0.565 with a standard deviation of 0.161. The average values of the daily clearness index range between 0.423 in January to 0.679 in July. The annual number of cloudy days is 44.4 (12.16%), the respective

number for partially cloudy days is 172.6 (47.29%) and 148 days are classified as clear days representing the 40.55% of the annual number of days. As it can be seen the summer months are classified mainly as clear days. The results of the partition of the daily global, PARE radiation and sunshine duration values on the basis of the corresponding K_r values (i.e., the criteria for classifying day type) are reported in Table 7. The annual mean of PARE_d is 2.4 MJ/m² for cloudy conditions, 5.9 MJ/m² for partly cloudy and 9.3 MJ/m² for clear sky conditions. The respective annual mean daily values of PPFD_d are 11.2 mol/m², 26.8 mol/m² and 42.7 mol/m². The annual daily average of sunshine duration is 7.0 hours with an annual total of 2555 hours. The monthly mean daily values range between 3.4 hours in January to 10.3 hours in July. The maximum daily value is 11.7 hours and it occurs in the summer months. The site is exposed to an average of about 57% of daily sunshine over the year.

Table 6: Monthly statistics of daily clearness index and number of days (N) according to the classification for each month of the year.

Month	N	Clearness Index (K _r)								Cloudy (K _r ≤ 0.35)		Partly Cloudy (0.35 < K _r < 0.65)		Clear (K _r ≥ 0.65)	
		Mean	StDev	CV (%)	Min	Q1	Median	Q3	Max	N	Percent	N	Percent	N	Percent
1	155	0.423	0.175	41.25	0.030	0.276	0.417	0.587	0.753	11.8	3.23	16.0	4.38	3.2	0.88
2	140	0.481	0.173	35.86	0.043	0.353	0.491	0.632	0.741	6.8	1.86	14.8	4.05	6.4	1.75
3	155	0.554	0.173	31.11	0.065	0.458	0.587	0.693	0.767	4.6	1.26	14.6	4.00	11.8	3.23
4	150	0.590	0.158	26.74	0.219	0.493	0.634	0.726	0.778	4.2	1.15	12.0	3.29	13.8	3.78
5	155	0.598	0.142	23.73	0.202	0.482	0.647	0.719	0.778	2.0	0.55	13.8	3.78	15.2	4.16
6	150	0.622	0.118	18.93	0.354	0.522	0.675	0.728	0.763	0.0	0.00	13.8	3.78	16.2	4.44
7	155	0.679	0.080	11.74	0.344	0.647	0.713	0.735	0.760	0.2	0.05	8.0	2.19	22.8	6.25

8	155	0.651	0.091	13.91	0.358	0.590	0.679	0.723	0.756	0.0	0.00	12.0	3.29	19.0	5.21
9	150	0.625	0.115	18.37	0.300	0.548	0.678	0.714	0.752	0.6	0.16	13.2	3.62	16.2	4.44
10	155	0.575	0.134	23.34	0.100	0.483	0.599	0.694	0.766	2.2	0.60	16.8	4.60	12.0	3.29
11	150	0.521	0.144	27.67	0.137	0.440	0.544	0.647	0.715	4.2	1.15	18.8	5.15	7.0	1.92
12	155	0.456	0.161	35.42	0.056	0.350	0.471	0.599	0.691	7.8	2.14	18.8	5.15	4.4	1.21
Year	1825	0.565	0.161	28.44	0.030	0.465	0.610	0.703	0.778	44.4	12.16	172.6	47.29	148.0	40.55

Table 7: Monthly statistics of daily global (G_d) (MJ/m^2), $PARE_d$ radiation (MJ/m^2), Photon Photosynthetic Flux Density ($PPFD_d$) (mol/m^2) and sunshine duration (S_d) (hrs/d) for clear, partially cloudy and cloudy days at Farmakas. N is the number of days according to the above classification for the period of measurements.

Cloudy		G_d (MJ/m^2)				$PPFD_d$ ($mol/m^2/d$)				$PARE_d$ (MJ/m^2)				S_d (hrs/d)			
Month	N	Mean	StDev	Med	Max	Mean	StDev	Med	Max	Mean	StDev	Med	Max	Mean	StDev	Med	Max
1	59	4.3	1.41	4.5	6.8	8.3	2.51	8.6	12.8	1.8	0.55	1.9	2.8	1.0	0.82	0.8	2.7
2	34	5.7	1.89	6.1	8.7	10.8	3.40	11.5	16.0	2.4	0.74	2.5	3.5	1.3	0.99	1.1	3.3
3	23	6.7	2.27	7.2	9.2	12.8	4.01	13.6	17.5	2.8	0.88	3.0	3.8	1.2	0.95	1.0	2.9
4	21	10.4	1.45	10.7	12.4	19.3	2.54	19.8	22.4	4.2	0.56	4.3	4.9	2.7	0.96	2.8	4.2
5	10	11.7	1.97	12.5	13.9	21.6	3.19	22.6	24.9	4.7	0.70	4.9	5.4	3.7	1.78	4.1	6.0
6																	
7	1	13.7	*	13.7	13.7	25.6	*	25.6	25.6	5.6	*	5.6	5.6	4.5	*	4.5	4.5
8																	
9	3	10.5	0.63	10.1	11.2	19.5	1.09	18.9	20.8	4.3	0.24	4.1	4.5	3.8	0.92	3.3	4.9
10	11	6.5	1.66	6.7	8.6	12.4	2.97	13.4	16.1	2.7	0.65	2.9	3.5	2.2	1.14	2.3	3.7
11	21	4.8	1.45	5.0	7.1	9.1	2.54	9.5	13.1	2.0	0.56	2.1	2.9	1.1	0.94	1.2	3.2
12	39	4.0	1.32	4.3	5.9	7.6	2.31	8.1	10.9	1.7	0.51	1.8	2.4	1.1	0.83	1.1	2.5
Year	222	5.9	2.84	5.5	13.9	11.2	5.13	10.4	25.6	2.4	1.12	2.3	5.6	1.5	1.23	1.3	6.0
P. Cloudy		G_d (MJ/m^2)				$PPFD_d$ ($mol/m^2/d$)				$PARE_d$ (MJ/m^2)				S_d (hrs/d)			
Month	N	Mean	StDev	Med	Max	Mean	StDev	Med	Max	Mean	StDev	Med	Max	Mean	StDev	Med	Max
1	80	9.3	1.76	9.4	12.3	16.6	2.89	16.9	21.4	3.6	0.63	3.7	4.7	4.6	1.30	4.5	7.1
2	74	11.5	2.27	11.6	16.4	20.6	3.78	20.8	29.1	4.5	0.83	4.6	6.4	4.8	1.45	4.8	7.9
3	73	15.7	2.36	16.1	21.4	27.9	3.94	28.3	37.7	6.1	0.86	6.2	8.3	6.1	1.34	6.2	9.5
4	60	19.4	3.06	19.3	24.3	34.3	5.18	34.3	42.4	7.5	1.13	7.5	9.3	7.3	1.60	7.1	10.1
5	69	20.4	3.42	20.4	26.1	36.5	5.96	36.2	46.9	8.0	1.31	7.9	10.3	7.3	1.84	7.2	11.1
6	69	21.2	3.13	21.4	26.7	38.3	5.51	38.4	49.4	8.4	1.21	8.4	10.8	7.5	1.53	7.9	10.3
7	40	23.2	2.55	23.4	26.7	42.4	4.43	43.2	48.4	9.3	0.97	9.5	10.6	8.4	1.30	8.6	10.4
8	60	20.7	2.72	21.2	25.3	37.9	4.95	38.7	46.7	8.3	1.08	8.5	10.2	7.8	1.38	8.1	10.0
9	66	16.7	2.62	16.7	22.1	30.5	4.63	31.0	40.1	6.7	1.01	6.8	8.8	6.6	1.31	6.5	9.2
10	84	13.1	2.23	13.0	18.1	23.6	3.84	23.6	32.6	5.2	0.84	5.2	7.1	5.7	1.19	5.7	8.5
11	94	10.2	1.74	10.0	13.4	18.0	2.96	17.8	23.7	3.9	0.65	3.9	5.2	5.0	1.30	4.9	7.5
12	94	8.4	1.52	8.3	11.3	14.9	2.41	14.9	19.5	3.3	0.53	3.3	4.3	4.3	1.33	4.4	6.8
Year	863	14.9	5.48	14.3	26.7	26.8	9.91	25.7	49.4	5.9	2.17	5.6	10.8	6.0	1.90	6.0	11.1
Clear		G_d (MJ/m^2)				$PPFD_d$ ($mol/m^2/d$)				$PARE_d$ (MJ/m^2)				S_d (hrs/d)			
Month	N	Mean	StDev	Med	Max	Mean	StDev	Med	Max	Mean	StDev	Med	Max	Mean	StDev	Med	Max
1	16	12.8	0.78	12.8	14.5	21.9	1.34	22.0	24.5	4.8	0.29	4.8	5.4	6.8	0.20	6.8	7.0
2	32	16.0	1.55	16.1	18.8	27.9	2.79	28.2	32.7	6.1	0.61	6.2	7.2	7.5	0.54	7.4	8.3
3	59	21.0	1.81	20.7	24.9	36.6	3.08	36.2	43.5	8.0	0.67	7.9	9.5	8.9	0.50	8.9	9.8
4	69	26.1	1.43	26.3	28.9	45.3	2.42	45.3	50.9	9.9	0.53	9.9	11.1	10.1	0.41	10.2	10.7
5	76	28.7	1.35	28.9	31.9	50.8	2.38	51.2	55.4	11.1	0.52	11.2	12.1	10.8	0.44	11.0	11.5
6	81	29.8	1.13	30.0	31.7	53.4	2.22	53.9	57.0	11.7	0.49	11.8	12.5	11.2	0.46	11.4	11.7

7	114	29.3	1.12	29.3	31.4	52.6	1.80	52.8	56.5	11.5	0.39	11.5	12.4	11.0	0.42	11.1	11.6
8	95	26.5	1.52	26.4	29.1	47.7	2.68	48.1	52.3	10.4	0.59	10.5	11.4	10.4	0.45	10.5	11.0
9	81	22.6	1.52	22.7	25.3	40.0	2.75	40.1	45.5	8.8	0.60	8.8	9.9	9.5	0.52	9.6	10.1
10	60	17.7	1.71	17.8	20.6	31.0	3.07	30.9	36.9	6.8	0.67	6.8	8.1	8.3	0.51	8.3	9.0
11	35	13.3	1.01	13.1	15.5	22.9	2.10	22.4	27.1	5.0	0.45	4.9	5.9	7.0	0.36	7.0	7.8
12	22	11.3	0.28	11.3	11.8	19.4	0.43	19.3	20.6	4.2	0.09	4.2	4.5	6.7	0.25	6.8	6.8
Year	740	24.1	5.76	25.9	31.9	42.7	10.62	46.0	57.0	9.3	2.32	10.1	12.5	9.7	1.47	10.1	11.7

The relationships of daily PAR radiation ($PARE_d$) and Photon Photosynthetic Flux Density ($PPFD_d$) with the daily global and sunshine duration are shown in the following equations. PARE radiation and global radiation are linearly related, while for the daily sunshine duration a second degree polynomial is used (Figure 14). All relationships have high coefficients of determination:

$$PARE_d = 1.390 * G_d \quad R^2 = 0.999 \quad (36)$$

$$PARD_d = 1.785 * G_d \quad R^2 = 0.999 \quad (37)$$

$$PARE_d = 1.730 + 0.325 * S_d + 0.049 * S_d^2 \quad R^2 = 0.916 \quad (38)$$

$$PPFD_d = 7.905 + 1.485 * S_d + 0.222 * S_d^2 \quad R^2 = 0.916 \quad (39)$$

Seasonal Variation of Daily PAR Indices: The time series

plots of the daily PAR and global radiation indices are shown in Figure 15. K_{PAR} and K_T show a similar pattern with the highest values occurring in the summer months. In contrast, $fPAR$ and $fFEC$ have their highest values in the winter months. The descriptive statistics of daily PAR indices for the three classes of sky conditions are presented in Table 8. The annual mean of K_{PAR} increases from 0.266 for cloudy conditions to 0.703 for clear sky conditions. Similarly, the relative sunshine duration (σ_s) increases from 0.132 to 0.764. In contrast, $fPAR_d$ decreases from 0.419 for cloudy conditions to 0.387 for clear sky conditions. A reduction is also observed for the fraction of photon flux density to energy conversion ($fFEC_d$). It decreases from 1.913 mol/MJ under cloudy conditions to 1.768 mol/MJ under clear sky conditions. This reduction is clearly illustrated in Figure 16. A similar graph is obtained between $fFEC_d$ and relative sunshine duration (σ_s). Daily K_{PAR} is closely related with the clearness index (K_T) and relative sunshine duration (σ_s):

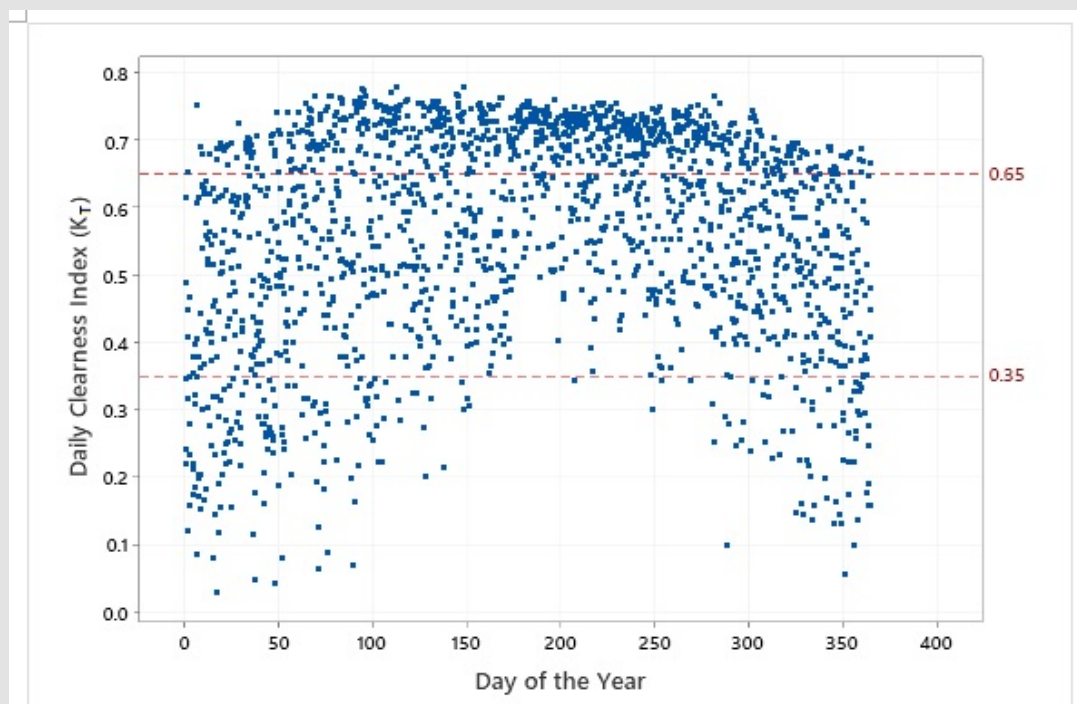


Figure 13: Daily clearness index (K_T) for each day of the year. The reference lines indicate the thresholds for the classification of the days according to the value of K_T .

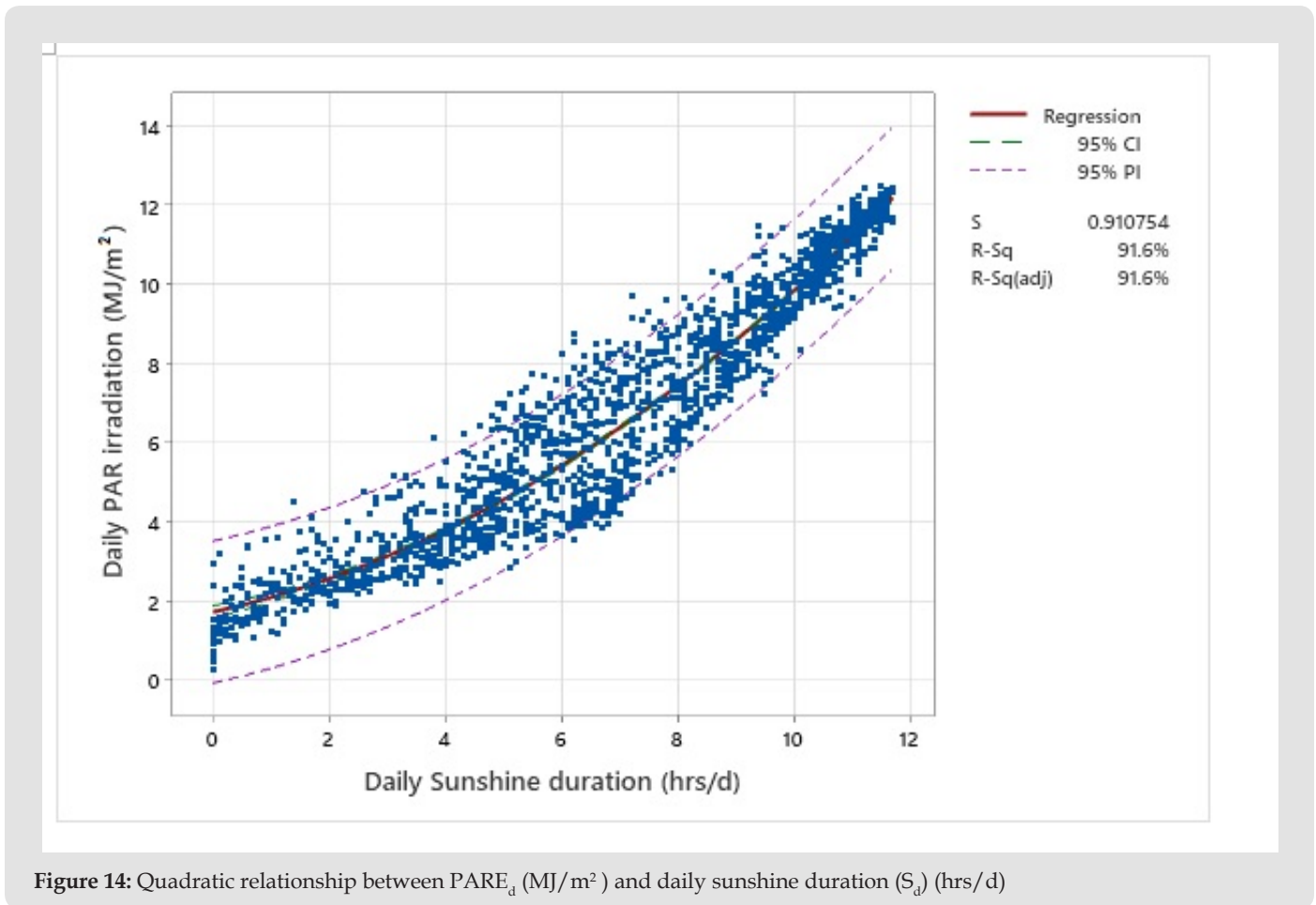


Figure 14: Quadratic relationship between $PARE_d$ (MJ/m²) and daily sunshine duration (S_d) (hrs/d)

Table 8: Descriptive statistics of daily PAR clearness index (K_{PAR}), fraction of PAR to global radiation ($fPAR_{\downarrow}$), fraction of photon flux to energy conversion ($fFEC_{\downarrow}$) and relative sunshine duration (od) under cloudy, partly cloudy and clear sky conditions for each month of the year

Month	Cloudy ($k_t \leq 0.35$)										Partly cloudy ($0.35 < K_t < 0.65$)										clear sky ($K_t \geq 0.65$)									
	PAR clearness Index (K_{PAR})					PAR clearness Index (K_{PAR})					PAR clearness Index (K_{PAR})					PAR Clearness Index (K_{PAR})														
	N	Mean	StDev	Min	Max	N	Mean	StDev	Min	Max	N	Mean	StDev	Min	Max	N	Mean	StDev	Min	Max	N	Mean	StDev	Min	Max					
1	59	0.254	0.074	0.037	0.259	0.368	0.081	0.372	0.512	0.630	16	0.503	0.081	0.372	0.512	0.630	0.662	0.026	0.626	0.656	0.747	0.662	0.026	0.626	0.656	0.747				
2	34	0.261	0.080	0.050	0.277	0.358	0.082	0.363	0.495	0.635	32	0.497	0.082	0.363	0.495	0.635	0.674	0.022	0.632	0.675	0.723	0.674	0.022	0.632	0.675	0.723				
3	23	0.246	0.081	0.080	0.266	0.340	0.072	0.375	0.529	0.641	59	0.525	0.072	0.375	0.529	0.641	0.693	0.031	0.614	0.694	0.743	0.693	0.031	0.614	0.694	0.743				
4	21	0.309	0.041	0.227	0.320	0.373	0.073	0.379	0.515	0.637	69	0.529	0.073	0.379	0.515	0.637	0.707	0.026	0.646	0.709	0.751	0.707	0.026	0.646	0.709	0.751				
5	10	0.303	0.043	0.224	0.317	0.341	0.082	0.368	0.513	0.659	76	0.512	0.082	0.368	0.513	0.659	0.710	0.031	0.636	0.715	0.757	0.710	0.031	0.636	0.715	0.757				
6							0.074	0.361	0.518	0.663	81	0.516	0.074	0.361	0.518	0.663	0.719	0.030	0.645	0.726	0.767	0.719	0.030	0.645	0.726	0.767				
7	1	0.359	*	0.359	0.359	0.359	0.060	0.420	0.591	0.665	114	0.584	0.060	0.420	0.591	0.665	0.724	0.022	0.670	0.730	0.763	0.724	0.022	0.670	0.730	0.763				
8							0.070	0.379	0.574	0.672	95	0.568	0.070	0.379	0.574	0.672	0.718	0.026	0.645	0.721	0.760	0.718	0.026	0.645	0.721	0.760				
9	3	0.343	0.026	0.313	0.356	0.360	0.081	0.365	0.549	0.664	81	0.541	0.081	0.365	0.549	0.664	0.706	0.022	0.654	0.709	0.754	0.706	0.022	0.654	0.709	0.754				
10	11	0.284	0.066	0.114	0.303	0.364	0.071	0.373	0.534	0.645	60	0.529	0.071	0.373	0.534	0.645	0.687	0.023	0.645	0.685	0.757	0.687	0.023	0.645	0.685	0.757				
11	21	0.267	0.066	0.157	0.271	0.355	0.074	0.352	0.520	0.646	35	0.518	0.074	0.352	0.520	0.646	0.655	0.020	0.623	0.648	0.697	0.655	0.020	0.623	0.648	0.697				
12	39	0.252	0.078	0.070	0.272	0.363	0.079	0.348	0.494	0.633	22	0.493	0.079	0.348	0.494	0.633	0.643	0.011	0.627	0.642	0.671	0.643	0.011	0.627	0.642	0.671				
Year	22	0.266	0.073	0.037	0.280	0.373	0.079	0.348	0.525	0.672	740	0.522	0.079	0.348	0.525	0.672	0.703	0.033	0.614	0.708	0.767	0.703	0.033	0.614	0.708	0.767				
	2										3																			
Month	Fraction of PAR ($fPAR_{\downarrow}$)										Fraction of PAR ($fPAR_{\downarrow}$)										Fraction of PAR ($fPAR_{\downarrow}$)									
	Mean	StDev	Min	Max	Mean	StDev	Min	Max	Mean	StDev	Min	Max	Mean	StDev	Min	Max	Mean	StDev	Min	Max	Mean	StDev	Min	Max	Mean	StDev	Min	Max		
	N	Mean	StDev	Min	Max	N	Mean	StDev	Min	Max	N	Mean	StDev	Min	Max	N	Mean	StDev	Min	Max	N	Mean	StDev	Min	Max	N	Mean	StDev	Min	Max
1	59	0.422	0.017	0.395	0.417	0.479	0.009	0.367	0.389	0.416	16	0.390	0.009	0.367	0.389	0.416	0.376	0.005	0.367	0.375	0.388	0.376	0.005	0.367	0.375	0.388				
2	34	0.421	0.020	0.395	0.415	0.484	0.008	0.373	0.391	0.409	32	0.392	0.008	0.373	0.391	0.409	0.381	0.005	0.368	0.382	0.390	0.381	0.005	0.368	0.382	0.390				
3	23	0.424	0.023	0.396	0.420	0.483	0.008	0.365	0.389	0.403	59	0.390	0.008	0.365	0.389	0.403	0.380	0.007	0.366	0.381	0.393	0.380	0.007	0.366	0.381	0.393				
4	21	0.407	0.010	0.384	0.410	0.420	0.008	0.361	0.388	0.406	69	0.387	0.008	0.361	0.388	0.406	0.381	0.006	0.367	0.381	0.390	0.381	0.006	0.367	0.381	0.390				
5	10	0.406	0.013	0.391	0.405	0.434	0.007	0.378	0.392	0.407	76	0.392	0.007	0.378	0.392	0.407	0.387	0.005	0.376	0.388	0.397	0.387	0.005	0.376	0.388	0.397				
6							0.010	0.375	0.398	0.415	81	0.396	0.010	0.375	0.398	0.415	0.392	0.006	0.375	0.392	0.405	0.392	0.006	0.375	0.392	0.405				
7	1	0.408	*	0.408	0.408	0.408	0.006	0.386	0.400	0.410	114	0.400	0.006	0.386	0.400	0.410	0.394	0.006	0.381	0.395	0.407	0.394	0.006	0.381	0.395	0.407				
8							0.006	0.387	0.400	0.414	95	0.400	0.006	0.387	0.400	0.414	0.395	0.006	0.379	0.396	0.408	0.395	0.006	0.379	0.396	0.408				
9	3	0.407	0.002	0.406	0.407	0.409	0.008	0.382	0.400	0.414	81	0.399	0.008	0.382	0.400	0.414	0.388	0.006	0.373	0.389	0.400	0.388	0.006	0.373	0.389	0.400				

Month	Photon Flux to Energy Conversion (ffEC _d)										Photon Flux to Energy Conversion (ffEC _d)									
	Mean	StDev	Min	Med	Max	Mean	StDev	Min	Med	Max	Mean	StDev	Min	Med	Max	Mean	StDev	Min	Med	Max
10	11	0.418	0.015	0.396	0.411	0.448	84	0.395	0.007	0.378	0.395	0.414	60	0.383	0.005	0.374	0.383	0.383	0.396	
11	21	0.417	0.012	0.398	0.415	0.446	94	0.389	0.008	0.371	0.389	0.412	35	0.377	0.008	0.364	0.377	0.377	0.394	
12	39	0.421	0.020	0.386	0.417	0.491	94	0.390	0.011	0.369	0.390	0.421	22	0.375	0.006	0.366	0.374	0.374	0.387	
Year	22	0.419	0.018	0.384	0.415	0.491	86	0.3	0.0	0.361	0.393	0.421	74	0.387	0.009	0.364	0.387	0.387	0.408	
	2						3	93	09				0							
Month	Relative Sunshine (σ _d)										Relative Sunshine (σ _d)									
	Mean	StDev	Min	Med	Max	Mean	StDev	Min	Med	Max	Mean	StDev	Min	Med	Max	Mean	StDev	Min	Med	Max
1	59	1.929	0.077	1.804	1.904	2.191	80	1.781	0.043	1.676	1.777	1.900	16	1.717	0.025	1.678	1.714	1.714	1.773	
2	34	1.922	0.091	1.805	1.896	2.210	74	1.791	0.036	1.702	1.787	1.871	32	1.743	0.023	1.683	1.745	1.745	1.783	
3	23	1.936	0.105	1.808	1.919	2.207	73	1.781	0.035	1.670	1.780	1.842	59	1.739	0.030	1.671	1.740	1.740	1.795	
4	21	1.861	0.047	1.753	1.874	1.921	60	1.770	0.036	1.651	1.771	1.855	69	1.740	0.026	1.678	1.743	1.743	1.781	
5	10	1.857	0.061	1.788	1.852	1.982	69	1.793	0.031	1.728	1.791	1.861	76	1.769	0.025	1.718	1.774	1.774	1.813	
6							69	1.811	0.044	1.715	1.817	1.896	81	1.790	0.028	1.712	1.793	1.793	1.849	
7	1	1.864	*	1.864	1.864	1.864	40	1.826	0.028	1.766	1.830	1.875	114	1.799	0.027	1.740	1.804	1.804	1.858	
8							60	1.829	0.028	1.769	1.826	1.890	95	1.803	0.026	1.733	1.808	1.808	1.863	
9	3	1.861	0.009	1.853	1.859	1.871	66	1.825	0.035	1.747	1.830	1.894	81	1.773	0.028	1.705	1.776	1.776	1.828	
10	11	1.909	0.070	1.810	1.878	2.047	84	1.805	0.033	1.726	1.803	1.891	60	1.750	0.024	1.710	1.750	1.750	1.812	
11	21	1.905	0.056	1.821	1.898	2.040	94	1.778	0.036	1.696	1.779	1.883	35	1.725	0.039	1.661	1.723	1.723	1.799	
12	39	1.923	0.091	1.765	1.908	2.242	94	1.783	0.051	1.688	1.781	1.930	22	1.715	0.029	1.673	1.707	1.707	1.770	
Year	22	1.913	0.082	1.753	1.896	2.242	86	1.7	0.0	1.651	1.794	1.930	74	1.768	0.039	1.661	1.769	1.769	1.863	
	2						3	95	42				0							
Month	Relative Sunshine (σ _d)										Relative Sunshine (σ _d)									
	Mean	StDev	Min	Med	Max	Mean	StDev	Min	Med	Max	Mean	StDev	Min	Med	Max	Mean	StDev	Min	Med	Max
1	59	0.098	0.082	0.000	0.082	0.269	80	0.460	0.130	0.185	0.443	0.706	16	0.679	0.022	0.618	0.684	0.684	0.704	
2	34	0.117	0.092	0.000	0.104	0.307	74	0.448	0.134	0.189	0.449	0.731	32	0.699	0.043	0.585	0.692	0.692	0.754	
3	23	0.101	0.082	0.000	0.085	0.246	73	0.514	0.114	0.255	0.521	0.792	59	0.760	0.032	0.677	0.772	0.772	0.799	
4	21	0.210	0.076	0.008	0.219	0.324	60	0.560	0.119	0.305	0.552	0.786	69	0.786	0.024	0.704	0.794	0.794	0.809	

5	10	0.266	0.125	0.044	0.297	0.426	69	0.528	0.132	0.271	0.535	0.794	76	0.780	0.031	0.663	0.793	0.811
6							69	0.525	0.107	0.335	0.551	0.718	81	0.784	0.032	0.656	0.794	0.817
7	1	0.324	*	0.324	0.324	0.324	40	0.599	0.092	0.384	0.621	0.736	114	0.783	0.028	0.657	0.794	0.813
8							60	0.585	0.103	0.316	0.611	0.740	95	0.782	0.029	0.683	0.794	0.809
9	3	0.313	0.073	0.263	0.280	0.397	66	0.539	0.110	0.323	0.531	0.758	81	0.778	0.030	0.602	0.788	0.800
10	11	0.195	0.102	0.036	0.203	0.336	84	0.518	0.106	0.279	0.507	0.756	60	0.744	0.030	0.644	0.751	0.778
11	21	0.113	0.091	0.000	0.121	0.314	94	0.492	0.127	0.182	0.486	0.717	35	0.692	0.028	0.607	0.690	0.743
12	39	0.112	0.086	0.000	0.114	0.259	94	0.448	0.137	0.207	0.456	0.705	22	0.688	0.025	0.591	0.696	0.705
Year	222	0.132	0.101	0.000	0.124	0.425		0.510	0.128	0.182	0.510	0.794	74	0.764	0.044	0.585	0.784	0.817
													0					

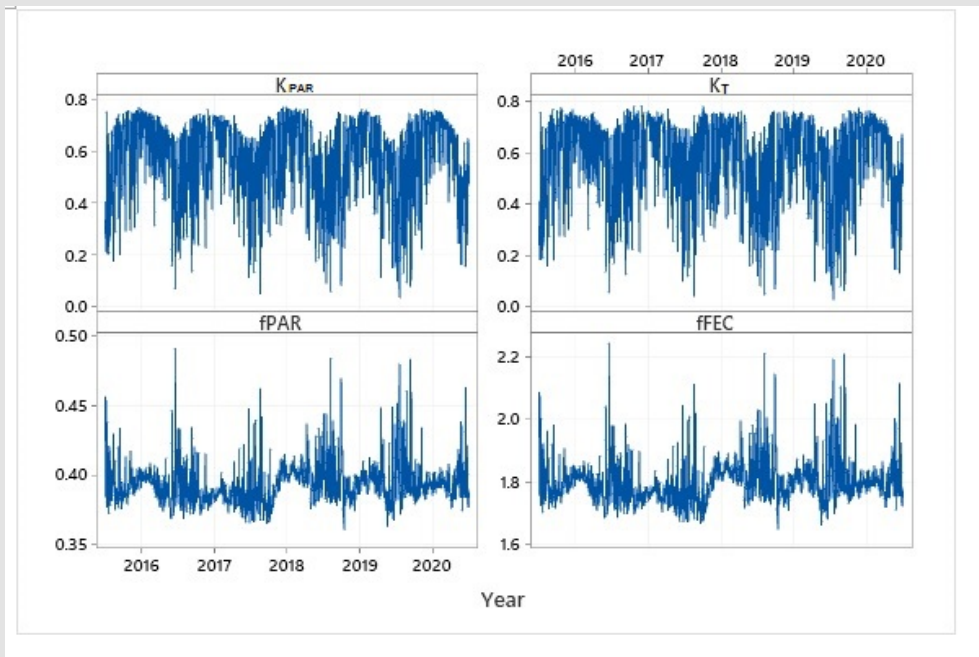


Figure 15: Time series plots of daily K_{PAR} , K_T , $fPAR$ and $fFEC$ indices of Farmakas

$$K_{PAR} = 0.027 + 0.952 * K_T \quad R^2 = 0.93 \quad (40)$$

$$K_{PAR} = 0.165 + 0.668 * \sigma_d \quad R^2 = 0.95 \quad (41)$$

The variability of all the daily indices is shown in Figure 17. The maximum of K_{PAR} and K_T are recorded in the summer months, while $fPAR$ and $fFEC$ are relatively constant throughout the year with the highest values occurring in the winter months. Outliers are also recorded mainly in the winter months. The frequency distributions of the above daily indices are shown through the histograms in Figure 18a. K_{PAR} and K_T show an exponential distribution, while $fPAR$ and $fFEC$ show an approximately normal distribution with mean values of 0.394 and 1.799 mol/MJ, respectively, respectively. The respective standard deviations of the said variables are 0.014 and 0.065 mol/MJ. The cumulative frequency curves of the above variables

are presented in Figure 18b. The reference line of 75% percentile is also shown. In 75% of days K_{PAR} and K_T are less than 0.695, $fPAR$ is less than 0.400 and $fFEC$ is less than 1.830 mol/MJ. The frequency distribution of $fFEC_d$ for each classification type of sky conditions is shown in Figure 18c. It is clear that in cloudy conditions $fFEC_d$ is higher than under clear conditions is shown in Figure 18c. It is clear that in cloudy conditions $fFEC_d$ is higher than under clear conditions.

The altitude dependency of the average annual values of daily $PPFD_d$ and $fFEC_d$ was checked with the help of the relevant values from a number of stations around the world. Figure 19 shows that $PPFD_d$ is increased with elevation while $fFEC_d$ is relatively constant with a very weak correlation. The slope is closed to zero and it is not significant at the 5% level. The values of Farmakas are closed to the regression lines.

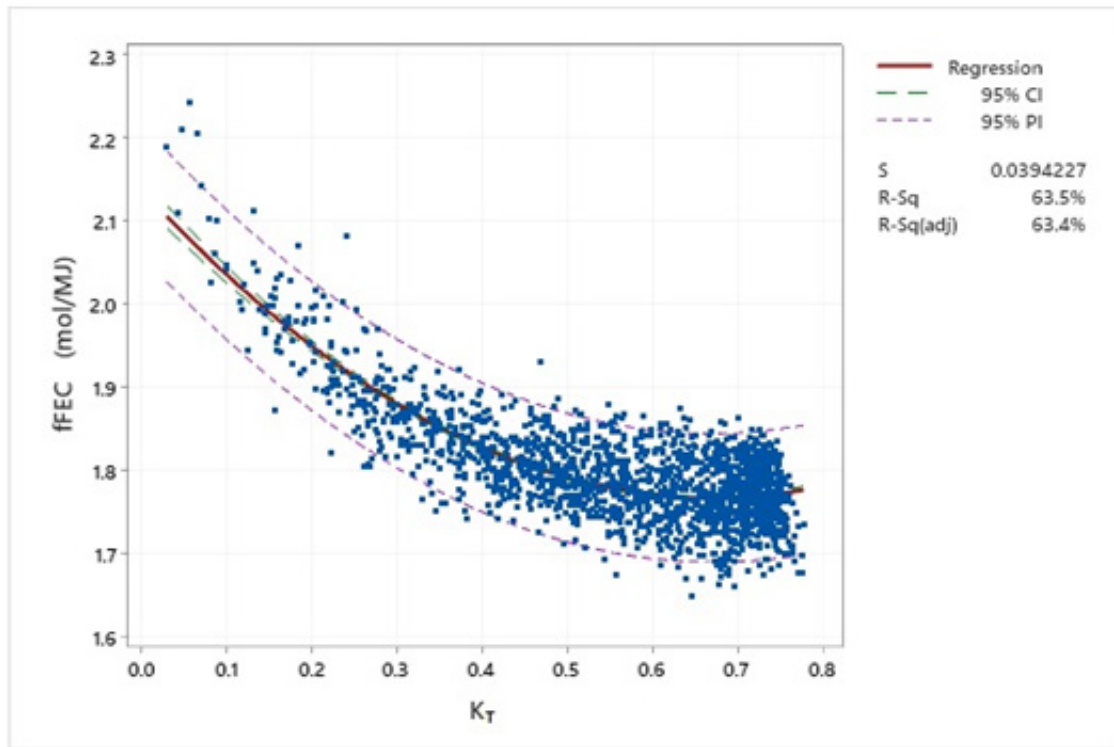


Figure 16: Relationship between the daily $ffEC_d$ and daily K_T index for Farmakas.

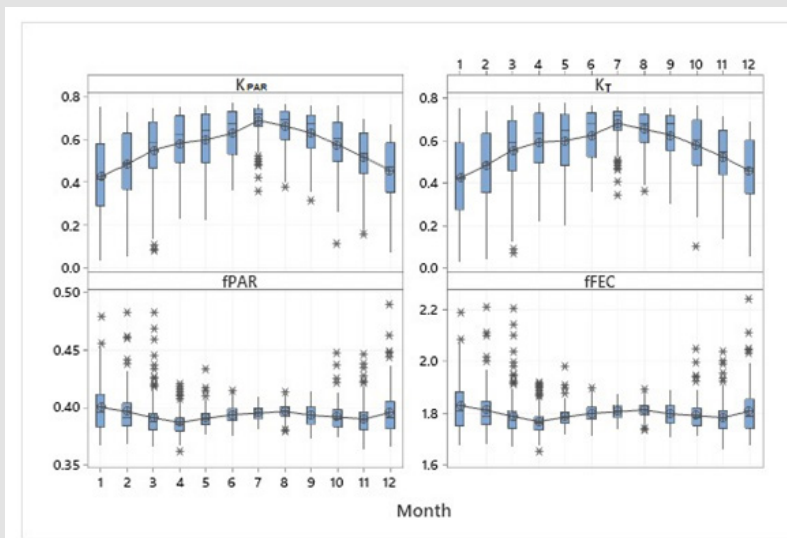


Figure 17: Boxplots of daily K_{PAR} , K_T , $fPAR_d$ and $ffEC_d$ for each month of the year.

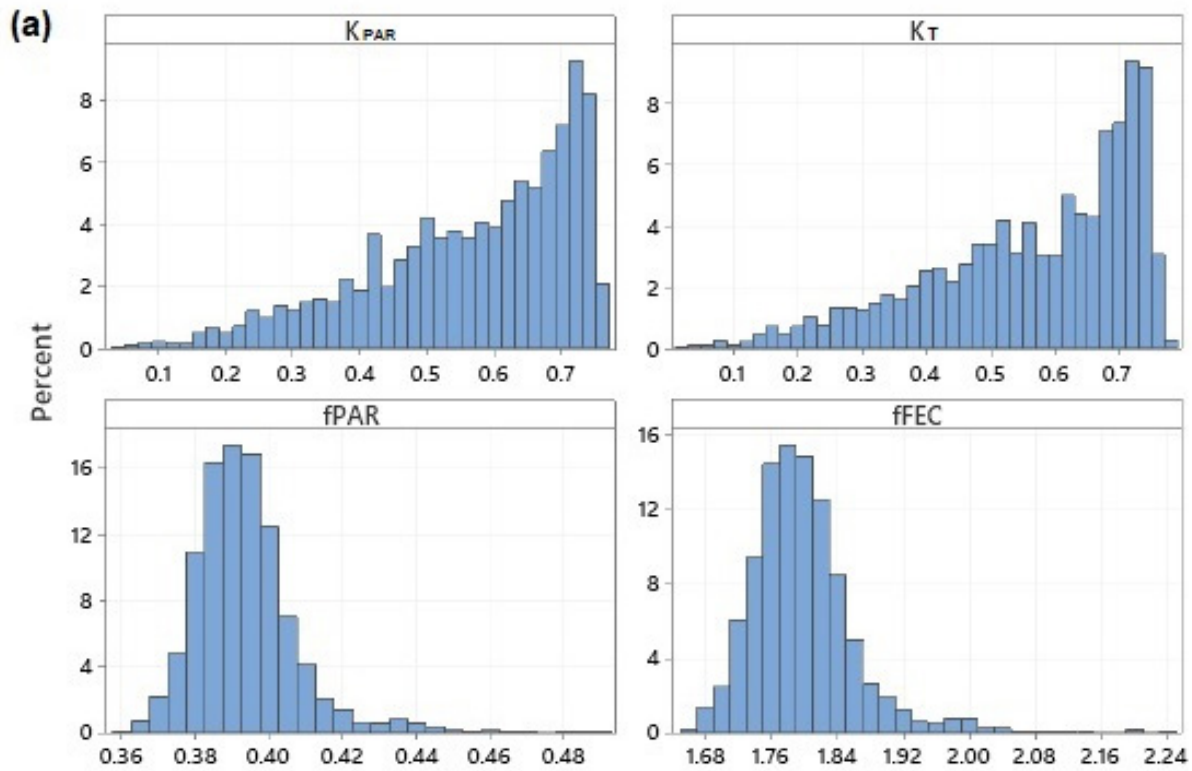


Figure 18a: Histograms of daily K_{PAR} , K_T , $fPAR$ and $ffEC$.

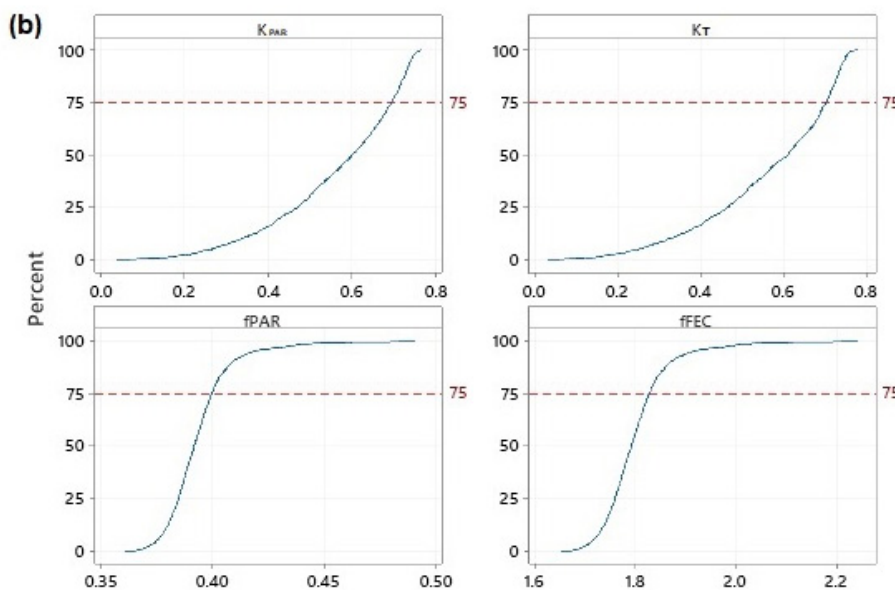


Figure 18b: Cumulative frequency function (CDF) of daily K_{PAR} , K_T , $fPAR$ and $ffEC$.

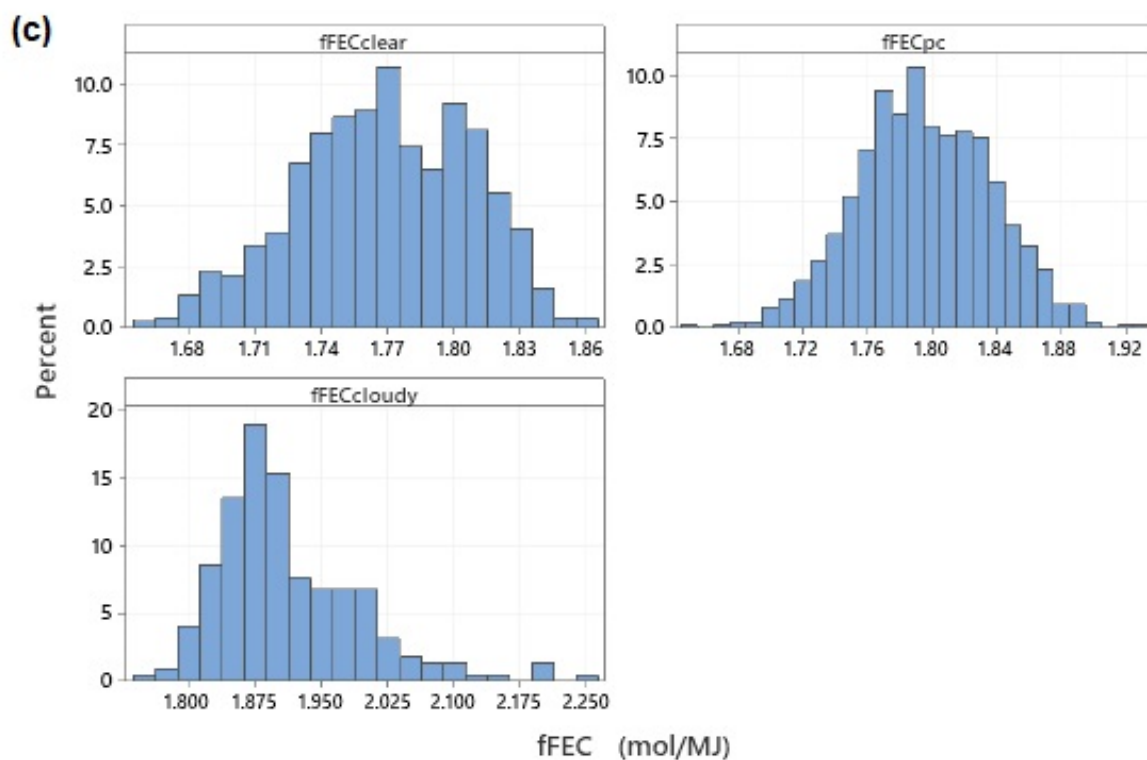


Figure 18c: Frequency distributions of $ffEC_d$ for each classification type according to sky conditions.

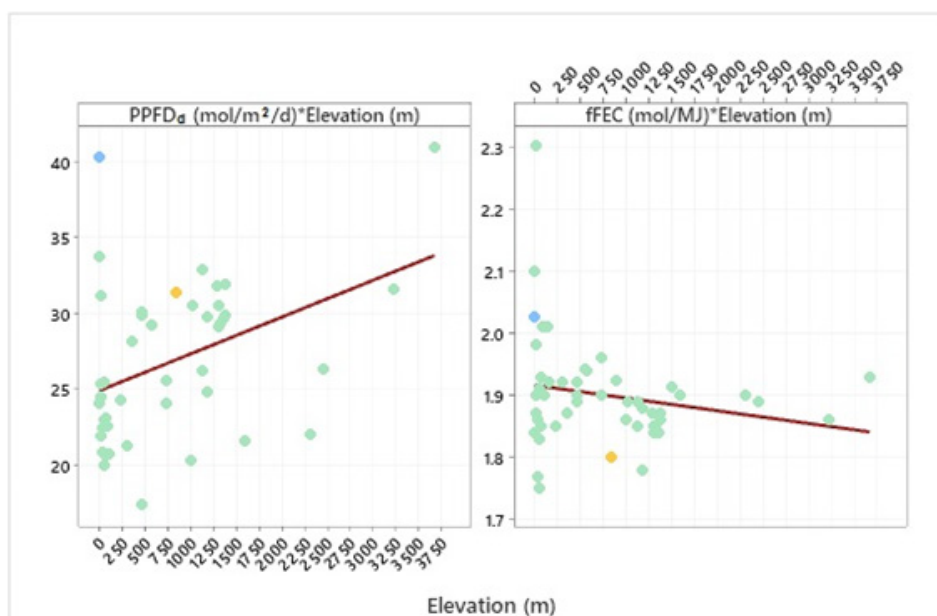


Figure 19: Relationship between $PPFD_d$ (mol/m²/d) and $ffEC_d$ (mol/MJ) with Elevation(m). Farmakas is shown with orange color and Larnaca (coastal station in Cyprus) with blue color.

Conclusions

Hourly data of global horizontal irradiance (G) and photosynthetic active radiation (PAR) were obtained from the automatic weather station of Farmakas, an inland location in Cyprus at the height of 833 m, covering the period 2016-2020. A CM-11 pyranometer is used for the measurement of global radiation in W/m^2 and a PAR-LITE Quantum Sensor for the measurement of PPFD flux in $\mu mol/s/m^2$. For the sunshine duration measurements, a Kipp & Zonen CSD3 sunshine duration sensor is used. The sensor, at the same time, measures the direct normal irradiance (B_n) in W/m^2 . PAR is either expressed as Photosynthetic Photon Flux Density (PPFD) in units of $\mu mol/s/m^2$ or in power units (PARE, W/m^2) which is more suitable for energy balance studies. From these units the following derived indices are calculated: (a) the fractional energy of PAR to global radiation (fPAR), (b) the fraction of photon flux energy conversion fFEC in $\mu mol/J$ for the hourly values and mol/MJ for the daily values and (c) the clearness index of PAR (k_{PAR}) i.e., the ratio PAR to the extraterrestrial one. Furthermore, these indices are related to the clearness index (k_t) which is the ratio of global radiation to the radiation at the top of the atmosphere. The first objective of the study is the quality assessment of the measured radiation components. For this purpose, the data were undergone an extensive quality control process for both the hourly and the daily values, which were then statistically analyzed including their derived indices. The BSRN tests showed that the data are within the specified limits. The second objective of the study refers to the modeling of PAR radiation using six models which differ in their complexity.

Monthly mean daily PPFD_d increased from 13.7 $mol/m^2/d$ in December to 49.8 $mol/m^2/d$ in July with annual mean value being 31.4 $mol/m^2/d$. Monthly mean daily fFEC_d increased from 1.77 mol/MJ in April to 1.83 mol/MJ in January with annual mean value being 1.80 mol/MJ . Similar values are obtained in most parts of the world. It was also discovered that partly cloudy skies (47.3%) were the dominant conditions which are followed by clear sky conditions (40.5%). Only 12.2% are considered as cloudy skies. Generally, fFEC_d is decreased from 1.91 mol/MJ under cloudy conditions to 1.77 mol/MJ under clear sky conditions, which is due to the strong absorption and scattering effects of clouds on longer wavelengths. Similarly, fPAR is decreased from 0.419 under cloudy conditions to 0.387 under clear sky conditions. The annual average of daily clearness index (K_t) is 0.565 with a standard deviation of 0.161.

Hourly values of global and PAR irradiances are shown by means of isolines diagrams. These values are considered representative of the solar radiation behavior along a typical year and can be useful for exploiting solar energy applications. Seasonal analysis allows in highlighting the difference between summer and winter irradiation conditions.

Six models different in their complexity are used to estimate

the PAR component. The simplest one was a linear relationship between PPFD and global irradiance, while the second and the sixth are multiple regression models based on global irradiance and clearness index and the cosine of solar zenith angle. The rest three models use power law equations based mainly on clearness index, optical air mass and cosine of solar zenith angle. The model coefficients were obtained from the four years 'training data set' (2016-2019) and the performance of the model was tested against the 'validation data set' of the year 2020, using the most popular statistical methods such as mean bias error (MBE), root mean square error (RMSE), relative percentage error (RE) and the coefficient of determination (R^2). The estimated parameters were close to those obtained by Hu et al. [33] in the North China plain. All models have high coefficient of determination. In all cases, the slopes of the regression lines between the estimated values and the measured ones are close to 1. With the exception of model C all other models show relatively low values of the statistical indicators of MBE, RMSE and RE. Therefore, the simple model A which is based on only one parameter (global radiation) and the empirical multilinear models B and F are essentially the best one.

The annual average daily global radiation intensity is around 17.5 MJ/m^2 , whereas PARE is 6.9 MJ/m^2 . The monthly mean daily values for the global radiation range between 7.5 and 27.5 MJ/m^2 while for PARE radiation they range between 3.0 and 10.9 MJ/m^2 . The maximum of daily global solar horizontal irradiation is reached in June or July and it is almost 32 MJ/m^2 . The daily maximum of PARE irradiation is 12.5 MJ/m^2 . The annual daily average sunshine duration is 7.0 hours with an annual total of 2555 hours. The monthly mean daily values of sunshine duration range between 3.4 hours in January to 10.3 hours in July. The maximum daily value is 11.7 hours and it occurs in the summer months. The site is exposed to an average of about 57% of daily sunshine over the year. The monthly mean daily relative sunshine duration ranges between 0.35 in January to 0.73 in July.

This work has specifically contributed to the characterization and analysis of hourly and daily solar photosynthetic active radiation and there derived indices.

Acknowledgments

The authors would like to thank the Meteorological Department of Cyprus for providing the solar radiation data used in this study.

References

- McCree KJ (1972a) Test of current definitions on photosynthetically active radiation. *Agric Meteorology* 10: 443-453.
- Monteith JL (1961) Climate variation and the plant growth of crops. *Quart JR Met Soc* 107:749-774.
- McCree KJ (1972b) Test of current definitions of photosynthetically active radiation against leaf photosynthesis data. *Agric. For. Meteorology* 10: 443-453.

4. Monteith JL (1973) Principles of Environmental Physics. Edward Arnold.
5. Penning de Vries FWT, Jansen DM, Ten Berge HFM, Bakema A (1989) Simulation of ecophysiological processes of growth in several annual crops. Pudoc Wageningen.
6. Joint Research Center (2004) The MARS Crop Yield Forecasting System. Methodology of the MARS Crop Yield Forecasting System. 1(4).
7. Landsberg JJ, Waring RH (1997) A generalized model of forest productivity using simplified concepts of radiation-use efficiency, carbon balance and partitioning. For Ecol Manag 95(3): 209-228.
8. Pei F, Li X, Liu X, Lao C (2013) Assessing the impacts of droughts on net primary productivity in China. J Environ Manag 114: 2362-2371.
9. Zhu XD, He HL, Liu M, Yu GR, Sun XM, et al. (2010) Spatio-temporal variation of photosynthetically active radiation in China in recent 50 years. J Geogr Sci 20: 803-817.
10. Peng S, Qingyun D, Lin A, Hu B, Xiao K, et al. (2015) Observation and estimation of photosynthetically active radiation in Lhasa (Tibetan Plateau). Advances in Space Research 55(6): 1604-1612.
11. Wang L, Gong W, Feng L, Lin A, Hu B, et al. (2015) Estimation of hourly and daily photosynthetically active radiation in Inner Mongolia, China, from 1990 to 2012. International Journal of Climatology 35: 3120-3131.
12. McCree K J (1973) The measurement of photosynthetically active radiation. Sol Energy 15(1): 83-87.
13. McCree K J (1972c) The action spectrum, absorptance and quantum yield of photosynthesis in crop plants. Agr And Forest Meteorology 9: 191-216.
14. Jacovides CP, Tymvios F S, Asimakopoulos DN, Steven MD (1997) Urban aerosol and clear skies spectra for global and diffuse photosynthetically active radiation. Agric. Forest Meteorology 87(2-3): 91-104.
15. Dye DG (2004) Spectral composition and quanta-to-energy ratio of diffuse photosynthetically active radiation under diverse cloud conditions. J Geophys Res 109: 1-12.
16. Papaioannou G, Papanikolaou N, Retalis D (1993) Relationships of photosynthetically active radiation and shortwave irradiance. Theor. Appl. Climatology 48: 23-27.
17. Jacovides CP, Tymvios FS, Asimakopoulos DN, Theofilou KM, Pashiardis S, et al. (2003) Global photosynthetically active radiation and its relationship with global solar radiation in the Eastern Mediterranean basin. Theor Appl Climatology 74: 227-233.
18. Alados I, Foyo-Moreno I, Alados-Arboledas L (1996) Photosynthetically active radiation: measurements and modeling. Agricultural and Forest Meteorology 78(1-2): 121-131.
19. Zhang XY, Zhang Y, Zhou Y (2000) Measuring and modeling photosynthetically active radiation in Tibet Plateau during April-October. Agric. For. Meteorology 102(2-3): 207-212.
20. Jacovides CP, Tymvios F S, Papaioannou G, Asimakopoulos DN, Theophilou CM, et al. (2004) Ratio of PAR to broadband solar radiation measured in Cyprus. Agric. Forest Meteorology 121(3-4): 135-140.
21. Hu B, Wang Y, Liu G (2007) Spatiotemporal characteristics of photosynthetically active radiation in China. J Geophys Res Atmos 112 (D14106).
22. Hu B, Wang YS (2012) The climatological characteristics of photosynthetically active radiation in arid and semi-arid regions of China. J Atmos Chem 69(2): 175-186.
23. Papaioannou G, Nikolidakis G, Asimakopoulos D, Retalis D (1996) Photosynthetically active radiation in Athens. Agric Forest Meteorology 81(3-4): 287-298.
24. Iqbal M (1983) An Introduction to Solar Radiation. Academic Press, Toronto.
25. Gueymard C (2004) The sun's total and spectral irradiance for solar energy applications and solar radiation models. Solar Energy 78: 423-453.
26. Jacovides CP, Tymvios FS, Asimakopoulos V D, Kaltsounides NA (2007) The dependence of global and diffuse PAR radiation components on sky conditions at Athens, Greece. Agric For Meteorology 143(3-4): 277-287.
27. Escobedo JE, Gomes EN, Oliveira AP, Soares J (2009) Modeling hourly and daily fractions of UV, PAR and NIR to global solar radiation under various sky conditions at Botucatu, Brazil. Appl Energy 86(3): 299-309.
28. Garcia Rodriguez A, Garcia-Rodriguez S, Diez Mediavilla M, Alonso Tristan C (2020) Photosynthetic Active Radiation, Solar Irradiance and the CIE Standard Sky Classification. Applied Sciences 10(22): 8007.
29. Alados I, Olmo FJ, Foyo-Moreno I, Alados-Arboledas L (2000) Estimation of photosynthetically active radiation under cloudy conditions. Agric. Forest Meteorology 102(1): 39-50.
30. Gueymard C (1989) Two band model for the calculation of clear sky solar irradiance, illuminance and photosynthetically active radiation of the earth's surface. Solar Energy 43, 253-265.
31. Jacovides C P, Tymvios FS, Boland J, Tsitouri M (2015) Artificial Neural Network models for estimating daily solar global, UV, PAR and broadband radiant fluxes in an eastern Mediterranean site. Atmospheric Research 152: 138-145.
32. Pinker RT, Laszio I (1992) Global distribution of photosynthetically active radiation as observed from satellites. J Clim 5: 56-65.
33. Hu B, Yangchun Y, Liu Z, Wang Y (2016) Analysis of photosynthetically active radiation and applied parameterization model for estimating of PAR in the North China Plain. J Atmos Chem 73(4): 345-362.
34. Alados I, Alados-Arboledas L (1999) Direct and diffuse photosynthetically active radiation: measurements and modeling. Agric. For. Meteorology 93(1): 27-38.
35. Wang L, Wei G, Yingying M, Hu B, Zhang M, et al. (2014) Photosynthetically active radiation and its relationship with global solar radiation in Central China. Int. J. Biometeorology 58: 1265-1277.
36. Pashiardis S, Kalogirou SA (2021) Assessment and statistical analysis of pyranometer and sunshine duration sensor's measurements by decomposing global radiation to its direct and diffuse components. Solar Energy and Sustainable Development 10(1): 34-64.
37. Pashiardis S, Kalogirou SA, Pelengaris A (2017) Characteristics of Photosynthetic Active Radiation (PAR) through statistical analysis at Larnaca, Cyprus. SM Journal of Biometrics & Biostatistics, 2(2): 1009.
38. Jacovides CP, Boland J, Asimakopoulos DN, Kaltsounides NA (2010) Comparing diffuse radiation models with one predictor for partitioning incident PAR radiation into its diffuse component in the eastern Mediterranean basin. Renewable Energy 35(8): 1820-1827.
39. Long CN, Shi Y (2008) An automated quality assessment and control algorithm for surface radiation measurements. Open Atmos Sci J 2: 23-37.
40. Tetens O (1930) Über einige meteorologische Begriffe. Z Geophys 6: 297-309.
41. Murray FW (1967) On the computation of saturation vapor pressure. J Appl Meteorology 6: 203-204.
42. Foyo-Moreno I, Alados I, Alados-Arboledas L (2017) A new conventional regression model to estimate hourly photosynthetic photon flux density under all sky conditions. Int J of Climatology 37(1): 1067-1075.
43. Mizoguchi Y, Yasuda Y, Ohtani Y, Watanabe T, Kominami Y, et al. (2014) A practical model to estimate photosynthetically active radiation using general meteorological elements in a temperate humid area and comparison among models. Theor Appl Climatology 115: 583-589.

44. Xia X, Li Z, Wang P, Cribb M, Chen H, Y Zhaoc (2008) Analysis of photosynthetic photon flux density and its parameterization in Northern China. *Agricultural and Forest Meteorology* 148(6-7): 1101-1108.
45. Bai JH (2012) Observations and estimations of PAR and solar visible radiation in North China. *J Atmos Chem* 69: 231-252.
46. Kasten F, Young AT (1989) Revised optical air mass tables and approximation formula. *Appl Opt* 28: 4735-4738.

ISSN: 2574-1241

DOI: 10.26717/BJSTR.2022.47.007502

A Pelengaris. Biomed J Sci & Tech Res



This work is licensed under Creative Commons Attribution 4.0 License

Submission Link: <https://biomedres.us/submit-manuscript.php>



Assets of Publishing with us

- Global archiving of articles
- Immediate, unrestricted online access
- Rigorous Peer Review Process
- Authors Retain Copyrights
- Unique DOI for all articles

<https://biomedres.us/>